Transgelin promotes ferroptosis to inhibit the malignant progression of esophageal squamous cell carcinoma

QIUYU CHEN[1*], LINGYUN ZHANG[1*], CHANGSHAN WAN[1*], BOLI YANG[1,2*], XIANGXU KONG[1], XIN XU[1], YU GU[1], CHEN WANG[1], XIAOTONG LIU[1], QIAN DING[1], LANPING ZHU[1], YING LI[3], BANGMAO WANG[1] and WEILONG ZHONG[1]

[1]Department of Gastroenterology and Hepatology, Tianjin Medical University General Hospital, Tianjin Institute of Digestive Diseases, Tianjin Key Laboratory of Digestive Diseases, Tianjin 300052; Departments of [2]Digestive Diseases and [3]Pathology, General Hospital of Jincheng, Jincheng, Shanxi 048006, P.R. China

Received October 22, 2022; Accepted February 24, 2023

DOI: 10.3892/ijo.2023.5524

Abstract. The aim of the present study was to examine the function of transgelin (TAGLN) and its underlying mechanism in the ferroptosis of esophageal squamous cell carcinoma (ESCC) cells. To meet this aim, the association between TAGLN expression and the prognosis of patients with ESCC was determined using tissue samples and clinical data. Gene Expression Omnibus databank and Gene Set Enrichment Analysis data were used to examine which genes were co-expressed with TAGLN, as well as the influence of TAGLN on ESCC. Subsequently, Transwell chamber, wound healing, Cell Counting Kit-8 viability and colony formation assays were performed to observe the effects of TAGLN on the migration, invasion, viability and proliferation of Eca-109 and KYSE-150 cells. The interaction between TAGLN and p53 in the regulation of ferroptosis was detected using reverse transcription-quantitative PCR, co-immunoprecipitation and fluorescence co-localization assays, and a xenograft tumor model was established to examine the effect of TAGLN on tumor growth. The level of TAGLN expression in patients with ESCC was found to be low, compared with normal esophageal tissue, and a positive association was identified between the prognosis of ESCC and TAGLN expression. The expression of the ferroptosis marker protein, glutathione peroxidase 4, was found to be high, whereas that of acyl-CoA synthetase long-chain family member 4 was lower in patients with ESCC compared with expression levels in healthy patients. The overexpression of TAGLN resulted in a significant decrease in the invasive and proliferative capabilities of Eca-109 and KYSE-150 cells *in vitro* compared with the control group; *in vivo*, TAGLN overexpression was found to significantly decrease tumor size, volume and weight after one month of growth. In addition, the proliferation, migration and invasion of Eca-109 cells *in vivo* was stimulated by the knockdown of TAGLN. The results of the transcriptome analysis further demonstrated that TAGLN was able to induce ferroptosis-associated cell functions and pathways. Finally, TAGLN overexpression was found to promote ferroptosis in ESCC through its interaction with p53. Taken together, the findings of the present study suggested that the malignant development of ESCC may be inhibited by TAGLN through the manifestation of ferroptosis.

Correspondence to: Professor Weilong Zhong or Professor Bangmao Wang, Department of Gastroenterology and Hepatology, Tianjin Medical University General Hospital, Tianjin Institute of Digestive Diseases, Tianjin Key Laboratory of Digestive Diseases, No. 154 Anshan Road, Heping District, Tianjin 300052, P.R. China
E-mail: zhongweilong@tmu.edu.cn
E-mail: mwang02@tmu.edu.cn

*Contributed equally

Abbreviations: ACSL4, acyl-CoA synthetase long-chain family member 4; Co-IP, co-immunoprecipitation; COX2, cyclooxygenase-2; EMT, epithelial-mesenchymal transition; ESCC, esophageal squamous cell carcinoma; FTH1, ferritin heavy chain 1; GEO, Gene Expression Omnibus; GO, Gene Ontology; GPX4, glutathione peroxidase 4; GSEA, Gene Set Enrichment Analysis; GSH, glutathione; KEGG, Kyoto Encyclopedia of Genes and Genomes; MDA, malondialdehyde; ROS, reactive oxygen species; TAGLN, transgelin; TCGA, The Cancer Genome Atlas; TF, transferrin

Key words: esophageal squamous cell carcinomas, ferroptosis, TAGLN, tumor invasion, tumor migration

Introduction

Esophageal cancer is one of the most common malignant tumors; in 2020, 604,100 new cases and 544,076 deaths were reported worldwide (1-3). Esophageal cancer is divided into esophageal squamous cell carcinoma (ESCC) and esophageal adenocarcinoma. ESCC forms from esophageal squamous epithelium, which accounts for the majority of esophageal cancer in China; esophageal adenocarcinoma is a malignant tumor that occurs from glands, with a relatively low proportion (4). ESCC is highly invasive, and undergoes lymph node metastasis. Patients with early esophageal cancer lack typical clinical symptoms and signs, whereas the middle and late

stages of the malignancy are associated with esophageal obstruction, lesion infiltration and metastasis, all of which have a detrimental effect on both the quality of life and the survival prognosis of patients (5). The main treatment methods for ESCC, including surgery, chemotherapy, radiotherapy and targeted therapies, have been widely promoted. The 5-year overall survival rate of patients with esophageal cancer is <30.3% (6). Even with improvements that have been made in terms of surgery and the development of multimodal therapies, the clinical outcome for patients remains unfavorable (7,8). Therefore, an exhaustive analysis of the origin of ESCC is necessary to identify novel therapeutic targets (9-14), and the underlying molecular mechanisms associated with the origin and invasion of ESCC also need to be investigated (15).

Ferroptosis is an oxidative, iron-dependent type of regulated cell death that is distinguished by excessive lipid peroxidation and iron accumulation, which results in oxidative damage to the cell membrane (16). Ferroptosis has been linked to tumor growth and therapeutic responses in various types of cancer (17). Tumor growth is dependent on the presence of iron, a trace element (18). In animal studies, increased iron accumulation was found to promote the occurrence of ferroptosis (19). Excess iron promotes the subsequent onset of lipid peroxidation through the iron-dependent Fenton reaction to generate reactive oxygen species (ROS) and to activate iron-containing enzymes, such as lipoxygenase (20,21). Glutathione peroxidase 4 (GPX4), an intracellular antioxidant enzyme, functions as a fundamental repressor of ferroptosis in cancer cells by directly reducing phospholipid hydroperoxide to hydroxy-phospholipid (22). The presence of lipid radicals and the depletion of glutathione (GSH) are among the biochemical phenomena that underlie ferroptosis (23,24). GPX4 catalyzes the reduction of lipid hydroperoxides into lipid alcohols by utilizing GSH as a reducing cofactor. This important antioxidant system (GSH-GPX4) functions to protect cells from ferroptosis. By contrast, acyl-CoA synthetase long-chain family member 4 (ACSL4) catalyzes the esterification of arachidonoyl and adrenoyl into phosphatidylethanolamines, and therefore has a role as an important contributor to ferroptosis (25,26). p53-mediated transcriptional inhibition of SLC7A11 (one of two subunits of system xc^-) has been shown to promote ferroptosis in cancer cells (16). Ferroptosis, therefore, serves a complex and a highly context-dependent role in tumor biology and therapy.

Transgelin (TAGLN; also known as SM22), an actin-binding protein, is mainly associated with cytoskeleton remodeling (27). In several types of tumor, such as prostate cancer, osteosarcoma and breast cancer, the expression level of TAGLN has been shown to be reduced, or even entirely deleted (28-30). An association between the expression of TAGLN and the occurrence, development and invasion of tumors has also been reported in several studies (31-33). A previous study showed that TAGLN may be involved in the migration of epithelial cells by interacting with actin or promoting podosome formation, and the downregulation of TAGLN expression could inhibit tumorigenicity and tumor growth *in vivo*, producing enhanced cytotoxic effects of metabolite anticancer drugs on pancreatic cancer cells (33). A recently published study demonstrated that cytoskeletal remodeling and malignant progression in colorectal cancer is regulated through the interaction of TAGLN with cartilage oligomeric matrix protein; this interaction was found to occur during epithelial-mesenchymal transition (EMT) (34). In addition, a previous publication by our research group demonstrated that the malignant progression of ESCC could be prevented by TAGLN through impeding EMT (35). However, to the best of our knowledge, to date relatively few studies have investigated the function of TAGLN in different types of tumors, or its association with ferroptosis.

Therefore, the present study aimed to examine the influence that TAGLN has on the invasive, metastatic and proliferative capabilities of ESCC cell lines through the regulation of ferroptosis. The function and underlying molecular mechanism of TAGLN in the incidence, development, invasion and metastasis of ESCC cells is also highlighted, and the potential therapeutic applications of TAGLN with respect to the identification and treatment of esophageal cancer are discussed.

Materials and methods

Clinical sample collection and information. Esophageal tissue samples from 25 patients with ESCC (age, 64.1±7.49) and 10 esophageal tissues from healthy controls (age, 63.58±8.76) were acquired from Tianjin Medical University General Hospital (Tianjin, China) between January 2021 and December 2022. Prior to the surgery, none of the patients had received any cancer treatment therapies. The last follow-up date was 31 October 2021. The 8th American Joint Committee on Cancer staging method was used to categorize the tumor stage and grade of the tissue samples (36). The present study was conducted according to the principles set out in The Declaration of Helsinki of the World Medical Association. Written informed consent was provided by each patient, and the Ethics Committee of Tianjin Medical University General Hospital approved the study (ethics no. IRB2021-WZ-134). The clinicopathological characteristics of the patients are presented in Table I.

Immunohistochemical analysis. Paraformaldehyde (4%) was used to fix the tissue specimens at room temperature for 24 h. The fixed paraffin-embedded tissue sections (4-μm thick) were subsequently dewaxed using xylene and hydrated through graded concentrations of ethanol in water. Sodium citrate buffer (0.01 mol/l) was used for antigen retrieval and the endogenous peroxidase activity was blocked by Enhanced Endogenous Peroxidase Blocking Buffer (cat. no. P0100A; Beyotime Institute of Biotechnology) at 37˚C for 20 min. The primary antibodies used for the immunohistochemical analysis were anti-TAGLN (1:100; cat. no. ab233971; Abcam), anti-GPX4 (1:200; cat. no. DF6701; Affinity Biosciences, Ltd.), anti-ACSL4 (1:400; cat. no. ab155282; Abcam), anti-p53 (1:800; cat. no. 60283-2-Ig; ProteinTech Group, Inc.), anti-cyclooxygenase-2 (COX2; 1:200; cat. no. abp51035; Abbkine Scientific Co., Ltd.), anti-transferrin (TF; 1:400; cat. no. 17435-1-AP; ProteinTech Group, Inc.) and anti-ferritin heavy chain 1 (FTH1; 1:800; cat. no. abp54401; Abbkine Scientific Co., Ltd.). These primary antibodies were added to the tissue sections and incubated at 4˚C overnight. Following a washing step using Immunol Staining Wash Buffer, Beijing Beyotime company, the tissue sections were incubated for

Table I. Data were analyzed by χ^2 to investigate the relationship between TAGLN expression and clinicopathological characteristics.

		TAGLN expression		
Clinicopathological characteristic	Cases, n=25	Negative	Positive	P-value
Sex				
Male	23	11	12	0.953
Female	2	1	1	
Age, year				
<65	14	6	8	0.562
≥65	11	6	5	
Tumor grade				
T1 + T2	4	0	4	0.036
T3 + T4	21	12	9	
Lymphatic invasion				
N0	7	1	6	0.035
N1-N3	18	11	7	
Differentiation				
High + moderate	12	6	6	0.8475
Low	13	6	7	
AJCC stage				
I-II	5	0	5	0.016
III-IV	20	12	8	
Size, cm				
<3	13	5	8	0.32
≥3	12	7	5	
Tumor site				
Upper and median	14	6	8	0.562
Lower	11	6	5	

AJCC, American Joint Committee on Cancer; TAGLN, transgelin.

30 min at 37˚C with the following HRP-conjugated secondary antibodies: Goat anti-mouse (1:500; cat. no. ab6789; Abcam) and goat anti-rabbit (1:1,000; cat. no. ab6721; Abcam). Horseradish peroxidase was then added, and the samples were further incubated at 37˚C for 20 min. The sections were scanned using a PRECICE 510B digital slice scanning system (Unic Technologies, Inc.), and observed by iViewer software (version 7.2.7.2; Unic Technologies, Inc.). The staining results were graded according to the staining intensity and percentage of positive cells. The cell staining intensity was scored as follows: 0, non-staining; 1, light yellow; 2, brownish yellow; and 3, yellowish brown. The percentages of positive cells were scored as follows: 0, <5%, 1, 5-25%; 2, 26-50%; 3, 51-75%; and 4, >75%. The positive intensity is the product of two scores: 0-2, negative; 3-5, weakly positive; 6-8, positive; and 9-12, strongly positive. Two pathologists assessed the findings independently, and the average values of five fields of view were used.

TAGLN expression analysis. The mRNA expression levels of TAGLN between the ESCC samples and normal tissues were compared using data acquired from the Gene Expression Omnibus (GEO) records (GSE161533, GSE45670 and GSE100942; http://www.ncbi.nih.gov/geo).

Gene Set Enrichment Analysis (GSEA). GSEA was completed using ESCC data obtained from The Cancer Genome Atlas (TCGA) project to identify the signaling pathways and biological phenomena that exert a role in the advancement of ESCC. The RNA-seq transcriptome data of ESCC patients in fragment per kilobase of transcript per million mapped reads format were extracted from TCGA. The average TAGLN transcript level was used to divide the patients with ESCC into high- and low-expression groups. For each assessment, gene set permutations were set to 1,000. The pathways enriched for each phenotype were classified according to the false discovery rate, nominal P-value and normalized enrichment score (NES). The DESeq algorithm for differential gene expression analysis was used, and the significance of DEGs was evaluated by $P<0.05$ and $|\log FC|>1$ (where FC is fold change) and were used as screening criteria. The R programming language was then used to generate volcano plots of the DEGs and to conduct clustering analysis. Volcano plots were generated using

ggplot2, a data visualization package in the R programming language. Specifically, the geom_point function was used to plot the log FC values against the negative logarithm of the adjusted P-values. Similarly, heatmaps were created using the R package heatmap, using the heatmap.2 function to display the relative expression levels of genes across different conditions. To investigate the biological roles of DEGs, biological process (BP) gene ontology (GO) enrichment analysis and molecular function (MF) GO term enrichment analysis based on the GO database (http://geneontology.org; accessed on April 5, 2022) was performed. Kyoto Encyclopedia of Genes and Genomes (KEGG) database (https://www.kegg.jp/kegg; accessed on April 5, 2022) analysis was performed for further assessment of the signaling pathways.

Culture of human ESCC cells. The human ESCC cell lines (KYSE-150 and Eca-109) were obtained from The Cell Bank of Type Culture Collection of The Chinese Academy of Sciences. Cells were cultured in RPMI-1640 medium containing 10% FBS (Gibco®; Thermo Fisher Scientific, Inc.) and maintained at 37˚C in an atmosphere of 5% CO_2.

Cell transfection. For cell transfection experiments, the Eca-109 and KYSE-150 cells were added at a density of $5x10^5$ cells/well into a 6-well plate. When confluency was 70-90%, cells were transfected using Lipofectamine 3000™ Transfection Reagent (Thermo Fisher Scientific, Inc.) following the manufacturer's guidelines. The TAGLN-overexpression plasmid (cat. no. HG14991-NY; TAGLN cDNA ORF Clone; human, pCMV3-N-HA as vector; Sino Biological) and an empty control plasmid (vector-NC; cat. no. CV017; pCMV3-N-HA as negative control vector; Sino Biological) were transfected into the KYSE-150 and Eca-109 cells. The final transfection concentration of plasmid was 100 nmol/l. After 6-8 h of culture in 10% serum medium without penicillin-streptomycin at 37˚C, the culture was replaced to 10% serum complete medium for 24-48 h.

To avoid off-target results, two different gene-specific siRNAs against TAGLN (si-TAGLN; one from Santa Cruz Biotechnology, Inc. (cat. no. sc-44163) and the other from Shanghai GenePharma Co., Ltd. (sense, 5'-GCUGAAGAA UGGCGUGAUUTT-3'; antisense, 5'-AAUCACGCCAUU CUUCSGCTT-3'), and the corresponding siRNA negative control (si-NC; cat no. sc-37007; Santa Cruz Biotechnology, Inc.) were transfected into KYSE-150 and Eca-109 cells, as aforementioned (using Lipofectamine 3000™; the final transfection concentration of siRNAs was 10 nmol/l). After culturing the cells at 37˚C in 10% serum medium without penicillin-streptomycin for 6-8 h, the medium was replaced with complete medium containing 10% FBS (cat. no. 10099141C; Gibco; Thermo Fisher Scientific, Inc.) and 1% penicillin-streptomycin (cat. no. 15140122; Gibco; Thermo Fisher Scientific, Inc.), and the cells were incubated for an additional 24-48 h prior to the follow-up experiments.

Experimental cells were separated into the following groups according to the nature of the transfections: si-NC, si-TAGLN-1, si-TAGLN-2, vector-NC (empty plasmid) and TAGLN overexpression plasmid. Subsequently, the cells were examined by Cell Counting Kit 8 (CCK-8) viability assay, EdU-labeling proliferation assay, colony formation assay, wound healing assay, and Transwell invasion and migration assays within 72 h after the completion of cell transfection.

CCK-8 assay. KYSE-150 and Eca-109 cells were seeded into a 96-well plate at a density of ~5,000 cells/well and cultured at 37˚C. After 24, 48 and 72 h, 10 μl CCK-8 reagent (Beyotime Institute of Biotechnology) was added to each well, and the cells were incubated at 37˚C for 1 h. A Tecan Infinite M200 Pro microplate analyzer (Tecan Group, Ltd.) was used to measure the absorbance of each well at 450 nm to calculate cell viability. Each experiment was repeated three times.

EdU-labeling proliferation assay. KYSE-150 and Eca-109 cells were seeded into 12-well plates at a density of $5x10^4$ cells/well and incubated in RPMI-1640 medium containing 10% FBS at 37˚C. The BeyoClick™ EdU-488 kit (Beyotime Institute of Biotechnology) was used to determine cell proliferation by examining DNA synthesis in the cells. EdU reagent (1 ml at 10 μM) was added to the cells and incubated at 37˚C for 60 min. The cells were fixed with 4% paraformaldehyde at room temperature for 15 min, and then treated with 1% Triton X-100 at room temperature for 15 min. Subsequently, 200 μl Click reaction solution was added to each well, and the cells were incubated in dark at room temperature for 30 min. Nuclei were stained with Hoechst (Beyotime Institute of Biotechnology). A Leica DM5000B fluorescence microscope (Leica Microsystems GmbH) was used to examine and capture images of the cells. Images were analyzed using LAS AF software v2.6.0.7266 (Leica Microsystems GmbH). The percentages of EdU-positive (DNA-replicating) and Hoechst-positive cells (total cells) were determined.

Colony formation assay. KYSE-150 and Eca-109 cells were seeded into a 6-well plate, at a range of densities between $2x10^2$ and $10x10^2$ cells/well, and cultivated in RPMI-1640 medium containing 10% FBS at 37˚C for 24 h. The cells were treated with various concentrations of Tanshinone I (Tan-I; Selleck Chemicals), 0, 1.2, 2.4, 4.8 and 9.6 μg/ml, prior to being resuspended in RPMI-1640 medium containing 10% FBS and cultured at 37˚C for 15 days in an atmosphere containing 5% CO_2 to stimulate colony formation; the medium containing 10% FBS was replaced every three days. The plate was washed using cold PBS and fixed with 4% paraformaldehyde solution. The fixed colonies were subsequently stained with 0.1% crystal violet for 30 min at room temperature. The number of visible colonies, those with a diameter >0.05 mm, was calculated using FIJI/ImageJ software (v2.1.0/1.53c; National Institutes of Health).

Wound healing assay. To prevent cell proliferation upon migration, the cells were allowed to rest overnight in serum-free medium prior to wound scratching. Digested cells were harvested and cultured (at a density of $2x10^5$ cells/well). Once the confluency of the cells had reached to 100%, wounds were made using a pipette tip. The wound closures were subsequently measured at 0, 12, 24 and 36 h to assess the degree of cell migration using a Nikon ECLIPSE Ts2 microscope (Nikon Corporation) and calculated using FIJI/ImageJ software (v2.1.0/1.53c; National Institutes of Health). Experiments were performed three times.

Transwell invasion and migration analysis. Matrigel™ (BD Biosciences) was diluted in RPMI-1640 medium containing 10% FBS after dissolution overnight at 4˚C. The mixture (50 μl) was added to the upper and the lower compartments of Costar® 24-well plates (cat. no. 3422; Corning, Inc.), which were then incubated at 37˚C for 30 min. Eca-109 and KYSE-150 cells in the exponential growth phase were collected; serum-free medium was used to wash and resuspend the cells to $5x10^4$ cells/ml. The bottom part of the Matrigel insert was merged in RPMI-1640 medium with 20% FBS, and cells were gently added to the upper compartment. Culture plates were then incubated at 37˚C with 95% relative humidity and in the presence of 5% CO_2 for 24 h, after which, the upper Transwell chambers were removed. The cells on the lower side of the insert were stained with 0.1% crystal violet for 15-30 min at room temperature, and images were captured for cell counting. The number of cells was counted in 10 fields, which were randomly selected using a Nikon ECLIPSE Ts2 microscope (Nikon Corporation), and the average numbers of cells were recorded. The Transwell migration assay was conducted as described above for the Transwell invasion experiment, but without Matrigel. Each experiment was repeated three times.

Xenograft tumor model. Four groups of female BALB/c nude mice (aged 4-6 weeks; n=24/group) were acquired from the SPF Beijing Biotechnology Co., Ltd. The mice were kept under pathogen-free conditions and provided sterile food and water *ad libitum*. The mice were raised in an environment with constant temperature of 20-26˚C, moderate humidity of 50-60% and a 12-h light/dark cycle. A total of $5x10^6$ cells in 100 μl PBS containing the TAGLN-overexpression vector, vector-NC, si-TAGLN or si-NC were subcutaneously inoculated into the right flank of the mice. Tumor growth was observed every 4 days. Following the procedure outlined in previous studies (37,38), transfection experiments were performed 10, 13 and 16 days after the injection of the tumor cells (designated as day 0). On days 10 and 13, 14 μg vector-NC or TAGLN-overexpression plasmids were combined with 21.7 μl Lipofectamine 3000™ Transfection Reagent (Thermo Fisher Scientific, Inc.); in addition, 434 pmol si-NC or si-TAGLN was mixed with 50 μl siRNA-Oligofectamine (Thermo Fisher Scientific, Inc.) to form a complex. The solutions are mixed with 5% dextrose water to a total volume of 100 μl. Following a period of incubation (10-15 min), an insulin syringe with a permanently attached needle was used to inject these reagent mixtures above into the tumor. On day 16, double doses of the siRNA and plasmid complexes were injected, and the amount of Oligofectamine was increased accordingly. This procedure was performed in accordance with the guidelines of the Animal Ethics Committee of Tianjin Medical University. The weight of the tumors in mice was not allowed to exceed 10% of their body weight, and the average tumor diameter never exceeded 15 mm. Mice and tumors were examined every 2-3 days; when the tumor exceeded 15 mm in diameter, the mice were euthanized. In case of ulceration, infection or necrosis, the experiment was terminated, and the mice were euthanized at that stage. On the 18th day of the experiment, one of the mice in the TAGLN knockdown group died; H&E staining was performed on their lungs and liver, and it was found that they had systemic metastasis. The remaining mice survived until the end of the experiment. At the end of the experiment, the mice were sacrificed and the tumors were removed. Mice were euthanized using the CO_2 method: Mice were placed into a cage, and 100% CO_2 was introduced at a flow rate of 30% CO_2 volume displacement/min. The CO_2 added to the chamber was allowed to reach equilibrium in the gas mixture to quickly realize the goal of animal unconsciousness and reduce animal pain. Animal death was confirmed by cardiac arrest, respiratory arrest, animal stiffness and dilated pupils. A 4% paraformaldehyde solution was used to fix the tumors at room temperature for 12-24 h, which were then submerged in paraffin and sectioned (4-μm thick) for later observation. The animal study was approved by the Ethics Committee of Tianjin Medical University General Hospital (ethics no. IRB2019-DWFL-414).

Reverse transcription-quantitative PCR (RT-qPCR) analysis. TRIzol™ (Invitrogen; Thermo Fisher Scientific, Inc.) was used to extract total RNA from the cells. cDNA was synthesized using a FastKing RT Kit with gDNase (cat. no. KR116; Tiangen Biotech Co., Ltd.) and amplified by qPCR using Applied Biosystems™ PowerUp™ SYBR™ Green Master Mix (cat. no. A25780; Thermo Fisher Scientific, Inc.), precisely following the manufacturer's instructions (Thermo Fisher Scientific, Inc.). The forward and reverse primer sequences were as follows: GAPDH forward, 5'-CCCTTCATTGACCTCAACTACATGG-3', and reverse 5'-CATGGTGGTGAAGACGCCAG-3'; TAGLN forward, 5'-GGTGGAGTGGATCATAGTGC-3', and reverse 5'-ATGTCAGTCTTGATGACCCCA-3'; GPX4 forward, 5'-ATGAAGATCCAACCCAAGGG-3', and reverse 5'-AGGTCCTTCTCTATCACCAGG-3'; ACSL4 forward 5'-CCAAAGAACACCATTGCCATC-3' and reverse 5'-AGCCTCAGATTCATTTAGCCC-3'; and p53 forward 5'-CCTCAGCATCTTATCCGAGTGG-3', and reverse 5'-TGGATGGTGGTACAGTCAGAGC-3'. The following PCR thermocycling conditions were used: 95˚C for 30 sec, 95˚C for 8 sec and 60˚C for 32 sec for 40 cycles; then 95˚C for 1 min, 60˚C for 30 sec and 95˚C for 30 sec. The relative expression of each of gene was calculated using the $2^{-\Delta\Delta Cq}$ method. Each sample was run in duplicate, and each experiment was repeated three times.

Western blot analysis. Tissues and cells were lysed using RIPA buffer (Beyotime Institute of Biotechnology) for total protein extraction. The BCA assay was used to quantify the total protein concentration. Proteins (40 μg) were separated using 12.5% SDS-PAGE gel, and the proteins were then transferred to a PVDF membrane using the wet (submersion) method (1 kDa/min). Subsequently, the membrane was blocked using 10% skimmed milk for 1 h at room temperature. After washing with TBS with 0.1% Tween-20, the membrane was incubated with the primary antibodies anti-TAGLN, anti-β-actin (cat. no. TA-09 ZSGB-BIO; OriGene Technologies, Inc.), anti-GAPDH (cat. no TA-08; ZSGB-BIO; OriGene Technologies, Inc.), anti-GPX4 and anti-ACSL4 antibodies (also see the *Immunohistochemical analysis* subsection above for further details) overnight at 4˚C. Note that the dilution ratio of the antibodies for western blot analysis was 1:1,000. The membrane was then washed and incubated with secondary antibodies, namely HRP-conjugated

goat anti-rabbit IgG (H+L) (cat. no. ZB-2301; ZSGB-BIO; ZSGB-BIO; OriGene Technologies, Inc.) and goat anti-mouse IgG (H+L) (cat. no. ZB-2305; ZSGB-BIO; ZSGB-BIO; OriGene Technologies, Inc.) for 1 h at room temperature. The proteins were visualized using an Enhanced Chemiluminescence (ECL) Western Blotting Substrate (cat. no. PE0010; Beijing Solarbio Science & Technology Co., Ltd.). Densitometric analysis was conducted using Image Lab software version 6.1 (Bio-Rad Laboratories, Inc.); each experiment was repeated three times.

Lipid peroxidation malondialdehyde (MDA) assay. Lipid peroxidation was detected in Eca-109 and KYSE-150 cells using a Lipid Peroxidation MDA Assay Kit (cat. no. BC0025; Beijing Solarbio Science & Technology Co., Ltd.), following the manufacturer's instructions. The cultured and transfected cells were collected and then subjected to ultrasonic fragmentation (power, 200 W; ultrasound 3 sec; interval, 10 sec; repeated 30 times), and the supernatant is centrifuged. MDA detection working solution was added and the mixture was incubated for 60 min in a 100˚C water bath; subsequently, then the mixture was centrifuged 8,000 x g at 4˚C for 10 min and 200 μl supernatant was added to each well of a 96-well plate for detection using a microplate analyzer to measure the absorbance of both the protein (at wavelength 450 nm) and MDA (at wavelengths of 532 and 600 nm).

GSH assay. GSH was measured in Eca-109 and KYSE-150 cells using a Reduced Glutathione (GSH) Colorimetric Assay kit (cat. no. E-BC-K030-M; Elabscience Biotechnology, Inc.), following the manufacturer's instructions.

ROS assay. The intracellular level of ROS was calculated by means of the fluorescent 2,7-dichlorofluorescein diacetate probe (Nanjing Jiancheng Bioengineering Institute), which was added to serum-free medium at a final concentration of 10 μM. The probe and Eca-109 and KYSE-150 cells ($5x10^6$) were then incubated for 30 min in the dark. The cells were washed twice with PBS to remove excess probe, and the fluorescence intensity was measured using a Tecan Infinite M200 Pro microplate analyzer (Tecan Group, Ltd.); the optimal excitation wavelength was 488 nm, and the optimal emission wavelength was 525 nm). Images of the cells were captured under a fluorescence microscope.

Iron and total iron assay. The level of Fe^{2+} or total iron in $5x10^6$ transfected Eca-109 and KYSE-150 cells was measured using the of Sigma-Aldrich Iron Assay kit (cat. no. MAK025; Merck KGaA) and a Tecan Infinite M200 Pro microplate analyze, following the manufacturer's instructions.

Fluorescence detection of Iron ions in living cells. Transfected Eca-109 and KYSE-150 cells ($5x10^4$) were inoculated in black polystyrene 96-well plates (cat. no. CLS3916; Corning, Inc.) and incubated overnight at 37˚C in a 5% CO2 incubator. The culture medium was removed and the cells were washed three times with serum-free RPMI-1640 medium. FerroOrange (cat. no. F374; Dojindo Laboratories, Inc.) was added at a 1 μmol/l working solution and the cells were incubated at 37˚C in a 5% CO_2 incubator for 30 min. Immediately following incubation, the cells were observed under a fluorescent microscope (Leica Microsystems GmbH).

Co-immunoprecipitation (Co-IP) assay. Co-IP was performed according to the instructions offered for each reagent in the process. Eca-109 cells ($1x10^7$) were lysed with Cell Lysis Buffer (cat. no P0013; Beyotime Institute of Biotechnology) and centrifuged at 13,000 x g for 15 min at room temperature. The anti-p53 antibody (1:100; cat. no. 10442-11-AP; Proteintech Group, Inc.), anti-TAGLN antibody (1:100; cat. no. ab233971; Abcam) and anti-rabbit IgG antibody (negative control) were incubated with 40 μg Protein A+G-Sepharose beads (cat. no. P2105; Beyotime Institute of Biotechnology) at 4˚C for 1 h. Each 1,000 μl extracted cellular protein sample was mixed with 40 μl of magnetic bead antibody mix and incubated for 2 h at room temperature. At the end of the incubation, the mixtures were placed on a magnetic stand for 10 sec to ensure separation, and the supernatant was removed. The beads were washed three times with a TBS, and 40 μg magnetic beads was added to 100 μl of protein loading buffer in a metal bath heated at 95˚C for 5 min, and then placed on the magnetic rack to remove the supernatant, leaving the target protein to be analyzed by western blotting.

Immunofluorescence co-localization assay. TAGLN-overexpressing Eca-109 cells ($1x10^4$) were seeded into 24-well plates and fixed for 10 min using 4% paraformaldehyde at room temperature. PBS containing 0.1% Triton X-100 was added for cell membrane permeabilization, and the cells were incubated for 10 min at room temperature. Then PBST containing 1% BSA (cat. no. A8020; Beijing Solarbio Science & Technology Co., Ltd.) was used for blocking at room temperature for 1 h. The cells were subsequently incubated with the primary antibodies, anti-TAGLN (1:100; cat. no. ab233971; Abcam), anti-p53 (1:100; cat. no. 10442 11 AP; Proteintech Group, Inc) and anti-HSPB1 (1:500; cat. no. ab109376; Abcam) and then carefully washed three times with PBS. Goat anti-,mouse IgG H&L (Alexa Fluor® 488-conjugated; 1:200; ab150113; Abcam) and donkey anti-rabbit IgG H&L (Alexa Fluor® 647-conjugated; 1:200; ab150075; Abcam) was used to stain the secondary antibodies. Nuclei were stained with DAPI (cat. no. S2110; Beijing Solarbio Science & Technology Co., Ltd.). Images of the cells were obtained using a laser-scanning confocal microscope (Leica Microsystems GmbH).

Comprehensive analysis of protein interactions. The protein-protein interaction (PPI) network information for TAGLN was downloaded from the Search Tool for the Retrieval of Interacting Genes/Proteins (STRING) website (version 11.0; https://string-db.org). Using the FerrDb dataset (version 1; http://www.zhounan.org/ferrdb), a total of 259 ferroptosis-associated genes were identified. Genes involved in the TAGLN and ferroptosis pathways were illustrated using a Venn diagram.

Statistical analysis. Statistical analysis was performed using GraphPad Prism 8.0 software (GraphPad Software; Dotmatics). All measurement data are shown as the mean ± standard deviation. Comparisons between two groups were analyzed using a two-tailed unpaired t-test, and multiple groups were

analyzed by one-way ANOVA followed by Tukey's post hoc test for further pairwise comparisons. Correlation analysis was performed using Pearson's correlation method, and the Kaplan-Meier followed by log-rank method was used to detect relevant associations between the expression levels of TAGLN and the subsistence prognosis of patients with ESCC. $P<0.05$ was considered to indicate a statistically significant difference.

Results

TAGLN expression level is lower in ESCC and is positively correlated with the prognosis of patients with ESCC. The respective endoscopic presentations of the normal esophageal tissue and ESCC are shown in Fig. 1A. The changes in TAGLN expression level in normal esophageal tissues and in ESCC tissues were distinguished using immunohistochemical analysis (Fig. 1B). The results showed that relative TAGLN expression was lower in ESCC compared with normal tissues (Fig. 1C). Statistical analysis confirmed that no significant associations were identified between the relative expression level of TAGLN in ESCC and age, sex, lymph node metastasis, tumor grade, tumor size, differentiation or tumor site of the patients (Table I). However, the relative expression of TAGLN was significantly associated with tumor grade, lymphatic invasion and AJCC stage (Table I). Moreover, the expression of ferroptosis-associated proteins, ACSL4 and GPX4, in ESCC and normal tissues was confirmed using immunohistochemistry, and the differences were found to be statistically significant (Fig. 1B and C). The correlation analyses were based on IHC stating scores; the expression of GPX4 was negatively correlated with TAGLN expression (Fig. 1E), whereas that of ACSL4 was positively correlated with TAGLN expression (Fig. 1F). The expression level of TAGLN was statistically higher in ESCC tissues at the early stages of cancer (stage IIa) compared with the advanced stages (stage III) (Fig. 1D); the difference between the expression of TAGLN in stage IIa and in the control groups was not statistically significant, whereas the differences between the expression of TAGLN in stage III groups and in the control group was identified as statistically significant. The differences between the expression of ACSL4 and GPX4 in ESCC stages IIa and stages III were found not to be statistically significant (Fig. 1D); however, the differences between the expression of ACSL4 and GPX4 in these two ESCC groups compared with expression in the control group were statistically significant.

The cut-off value used to separate patients into high and low expression groups was 3.7 (median value) according to IHC staining score. Kaplan-Meier analysis of the data demonstrated a significant association between the survival prognosis of patients with ESCC and the relative expression levels of TAGLN; that is, patients with high expression of TAGLN had a longer overall survival rate compared with patients with a low expression of TAGLN (Fig. 1G).

Subsequently, the expression levels of the ferroptosis-associated proteins p53, COX2, TF and FTH1 in ESCC and normal tissues were detected by immunohistochemical analysis. The differences in the expression of p35, COX2, TF and FTH1 between the ESCC and normal tissues were found to be statistically significant (Fig. 2A and B). The differences in the expression of p53, COX2, TF and FTH1 between ESCC stage III and normal tissues were found to be statistically significant. The differences in the expression of p53 and TF between ESCC stage IIa and normal tissues were not statistically significant, whereas the differences in the expression of COX2 and FTH1 between ESCC stage IIa and normal tissues were found to be statistically significant. The differences between the expression levels of p53, COX2, TF and FTH1 in ESCC stage IIa and stages III, however, were found not to be statistically significant (Fig. 2C). FTH1 expression was negatively correlated with TAGLN expression, whereas TF expression was positively correlated with TAGLN expression (Fig. 2D). However, the correlations between p53 and COX2 expression and TAGLN expression were found not to be statistically significant.

TAGLN expression level is decreased in ESCC and is associated with various cancer cell signaling pathways. TAGLN expression level is decreased in ESCC and is associated with various cancer cell signaling pathways (39). The GEO databank is a publicly accessible genomics data repository for high-throughput sequencing. The databank contains sequence and array based gene profile data, and was used in this study to profile the expression of genes in ESCC. Three datasets, GSE161533, GSE45670 and GSE100942, were used to examine the differential expression of TAGLN in ESCC and normal tissues. A significant decrease in the level of TAGLN expression in ESCC compared with expression in normal tissue was observed in these datasets (Figs. 3A-C and S1). Using the median TAGLN mRNA level as a cutoff value, the patients with ESCC in TCGA were split into high and low TAGLN subgroups. The signaling pathways and cellular processes that were significantly associated with the high TAGLN subgroup compared with the low TAGLN subgroup were identified by GSEA (Fig. 3D-I). Genes upregulated in the high TAGLN subgroup were mostly enriched in 'focal adhesion' (NES=2.01; $P<0.0001$), 'ECM receptor interaction' (NES=1.94; $P=0.002$), 'Gap junction' (NES=1.73; $P=0.004$), 'TGF-β signaling pathway' (NES=1.65; $P<0.05$) and 'Cell adhesion molecules (CAMS)' (NES=1.74; $P<0.05$). These pathways have been associated with tumor proliferation, invasion and other malignant progressions (40,41), suggesting that TAGLN may serve an important role in ESCC.

Overexpression of TAGLN attenuates ESCC cell proliferation, colony formation, invasion and migration. To determine whether TAGLN exerts a role in the malignant progression of ESCC, TAGLN was overexpressed in Eca-109 and KYSE-150 cell lines. The efficiency of mRNA and protein overexpression was confirmed using RT-qPCR and western blot analyses, respectively, and the mRNA and protein expression levels in TAGLN group were found to be significantly higher compared with the vector-NC (Fig. 4A and B). The CCK-8, EdU and colony formation assay results revealed that the overexpression of TAGLN in ESCC cell lines led to a significant reduction in the capability of the ESCC cells to proliferate (Fig. 4C-E). Compared with the control group, the number of migrating and invading cells was also significantly decreased (Fig. 4F) following the overexpression of TAGLN in both cell lines. The ability of the cells to migrate was also significantly reduced in the wound healing assay following

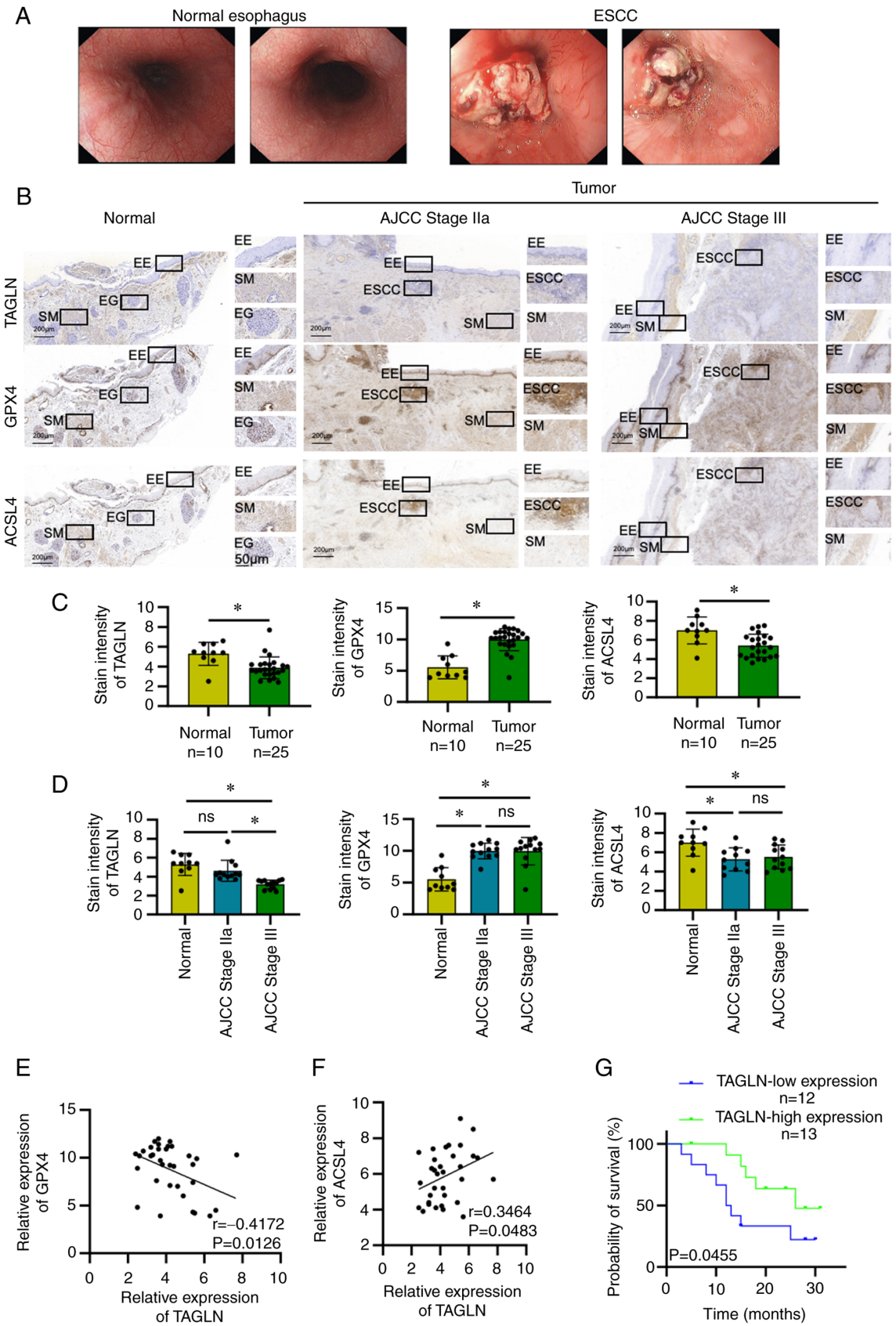

Figure 1. TAGLN expression in ESCC and its association with ESCC prognosis. (A) Relative endoscopic presentation of normal esophagus and that of patients with ESCC. (B) Immunohistochemistry was used to detect the expression of TAGLN, GPX4 and ACSL4 in normal esophageal tissues and in ESCC stages I-II and III-IV tumoral tissues. (C) Statistical analysis of TAGLN, GPX4 and ACSL4 expression in normal esophagus and ESCC tissues. Data are presented as the mean ± SD of three independent experiments. (D) Statistical analysis of the expression of TAGLN, GPX4 and ACSL4 in normal esophagus, stage I-II and III-IV ESCC tissues. Data are presented as the mean ± SD of three independent experiments. *P<0.05, as determined by two-tailed unpaired Student's t-test. Correlation between TAGLN and (E) GPX4 and (F) ACSL4 expression. (G) Survival curve of patients with ESCC with high and low TAGLN expression levels in cancer tissues. AJCC, American Joint Committee on Cancer; ACSL4, acyl CoA synthetase long chain family member 4; EE, esophageal epithelium; EG, esophageal gland; ESCC, esophageal squamous cell carcinoma; ns, not significant; SM, smooth muscle; TAGLN, transgelin.

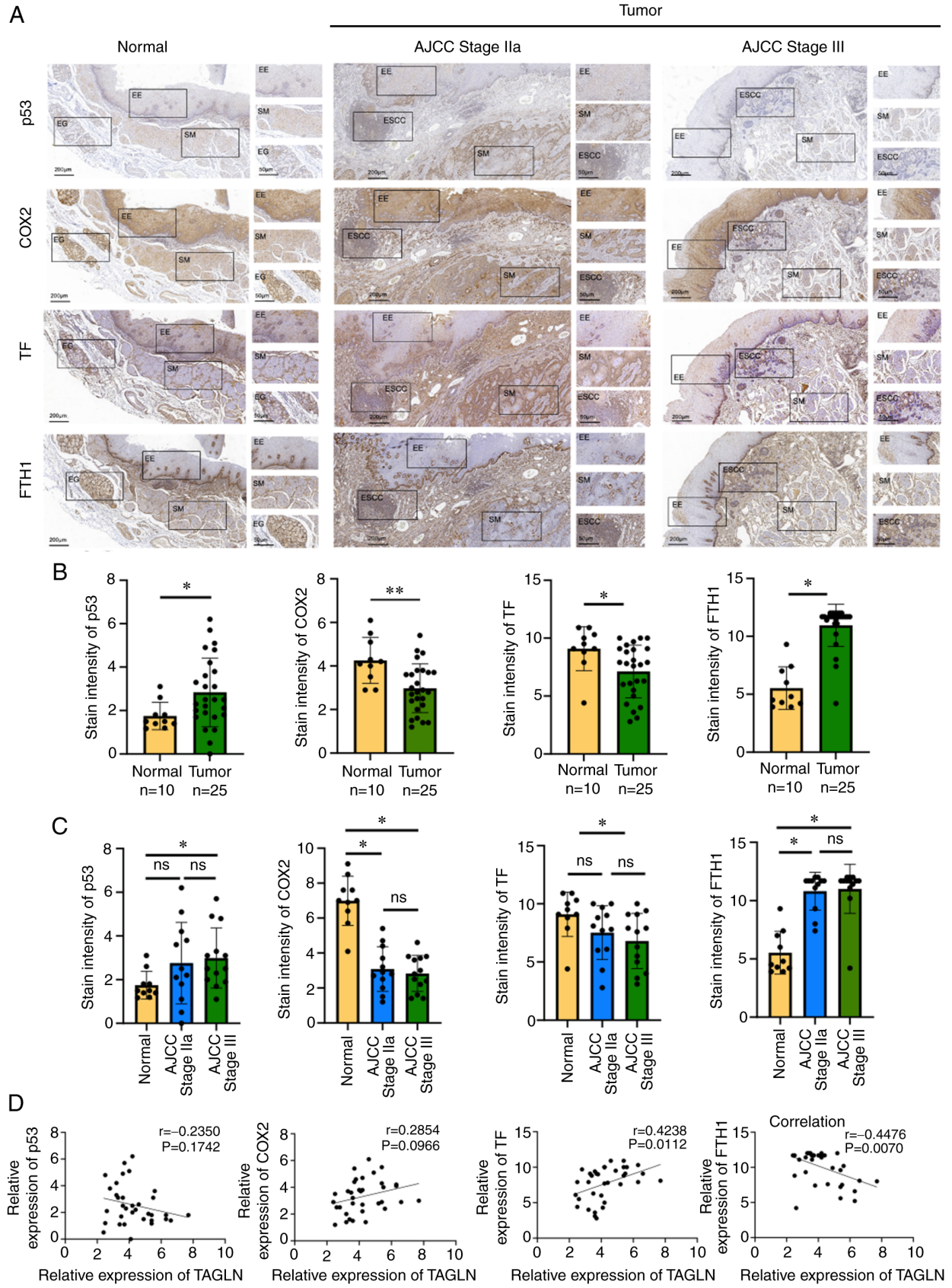

Figure 2. Ferroptosis-related protein expression levels in ESCC and their correlation with TAGLN. (A) Expression levels of p53, COX2, TF and FTH1 detected by immunohistochemistry in normal esophagus, stage I-II and III-IV ESCC tumor tissues. (B) Statistical analysis of the expression of p53, COX2, TF and FTH1 in normal esophagus and cancer tissues. Data are presented as the mean ± SD of three independent experiments. (C) Statistical analysis of the expression of p53, COX2, TF and FTH1 in normal esophagus, stage I-II and III-IV ESCC tumor tissues. Data are presented as the mean ± SD of three independent experiments. *P<0.05 and **P<0.01, as determined by two-tailed unpaired Student's t-test. (D) Correlation between p53, COX2, TF and FTH1 expression and TAGLN expression in normal esophagus and cancer tissues. AJCC, American Joint Committee on Cancer; COX2, cyclooxygenase 2; EE, esophageal epithelium; EG, esophageal gland; ESCC, esophageal squamous cell carcinoma; FTH1, ferritin heavy chain 1; ns, not significant; SM, smooth muscle; TAGLN, transgelin; TF, transferrin.

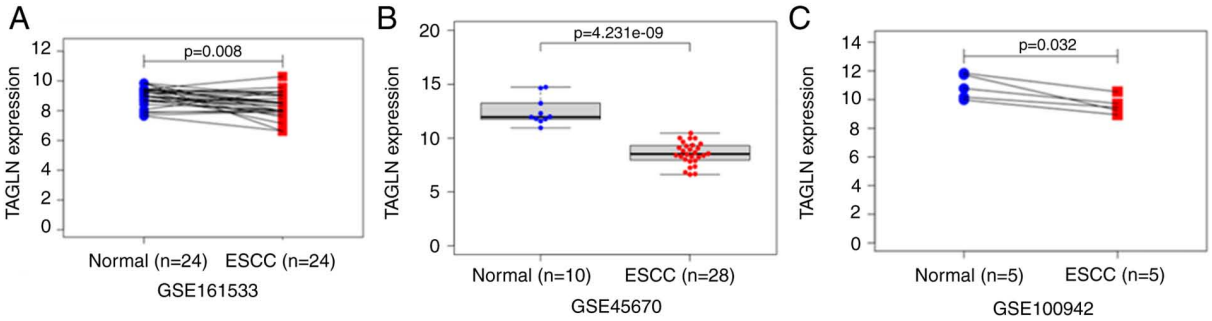

D Signaling pathways associated with TAGLN expression

	GS follow link to MSigDB	GS DETAILS	SIZE	ES	NES	NOM p-val	LEADING EDGE
1	KEGG_DILATED_CARDIOMYOPATHY	Details...	90	0.60	2.04	0.000	tags=47%, list=15%, signal=54%
2	KEGG_HYPERTROPHIC_CARDIOMYOPATHY_HCM	Details...	83	0.59	2.03	0.000	tags=41%, list=13%, signal=47%
3	KEGG_FOCAL_ADHESION	Details...	199	0.57	2.01	0.000	tags=38%, list=12%, signal=42%
4	KEGG_ECM_RECEPTOR_INTERACTION	Details...	84	0.67	1.94	0.002	tags=51%, list=14%, signal=59%
5	KEGG_VASCULAR_SMOOTH_MUSCLE_CONTRACTION	Details...	114	0.52	1.91	0.008	tags=33%, list=10%, signal=37%
6	KEGG_GLYCOSPHINGOLIPID_BIOSYNTHESIS_GANGLIO_SERIES	Details...	15	0.66	1.88	0.006	tags=33%, list=9%, signal=36%
7	KEGG_ARRHYTHMOGENIC_RIGHT_VENTRICULAR_CARDIOMYOPATHY_ARVC	Details...	74	0.55	1.85	0.006	tags=39%, list=13%, signal=45%
8	KEGG_CELL_ADHESION_MOLECULES_CAMS	Details...	131	0.49	1.74	0.032	tags=39%, list=21%, signal=49%
9	KEGG_GAP_JUNCTION	Details...	89	0.44	1.73	0.004	tags=28%, list=13%, signal=32%
10	KEGG_GLYCOSAMINOGLYCAN_BIOSYNTHESIS_CHONDROITIN_SULFATE	Details...	22	0.62	1.71	0.032	tags=64%, list=27%, signal=87%
11	KEGG_MELANOMA	Details...	71	0.44	1.70	0.002	tags=34%, list=17%, signal=40%
12	KEGG_TGF_BETA_SIGNALING_PATHWAY	Details...	85	0.43	1.65	0.012	tags=40%, list=23%, signal=52%

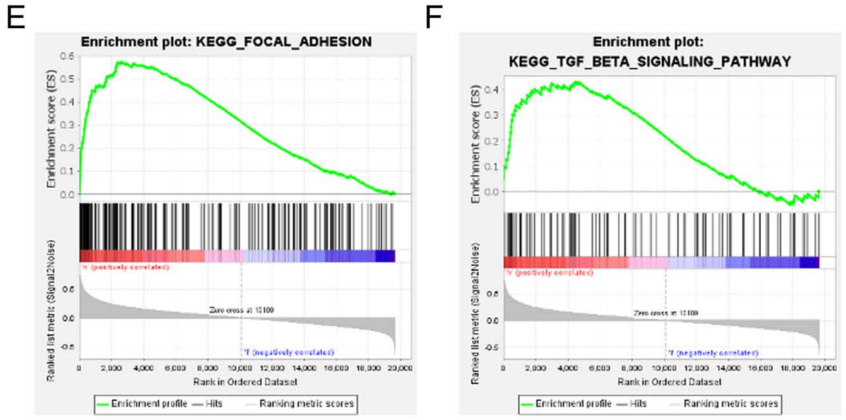

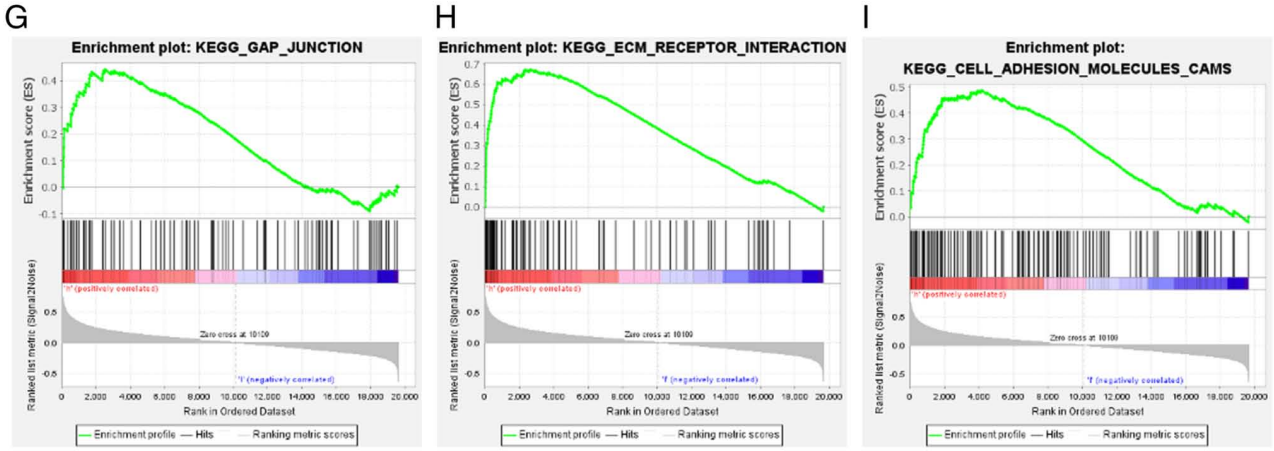

Figure 3. TAGLN expression is lower in ESCC and is associated with various cancer cell signaling pathways. Three datasets from the Gene Expression Omnibus, (A) GSE161533, (B) GSE45670 and (C) GSE100942 were used to validate the differential expression of TAGLN in ESCC tissues and normal tissues. (D) Signaling pathways associated with TAGLN expression in ESCC by KEGG. Genes upregulated in the TAGLN-high subgroup were enriched in (E) focal adhesion, (F) TGF-β signaling, (G) gap junction, (H) ECM receptor interaction, and (I) cell adhesion molecules (CAMS). ECM, extracellular matrix; ESCC, esophageal squamous cell carcinoma; KEGG, Kyoto Encyclopedia of Genes and Genomes; TAGLN, transgelin.

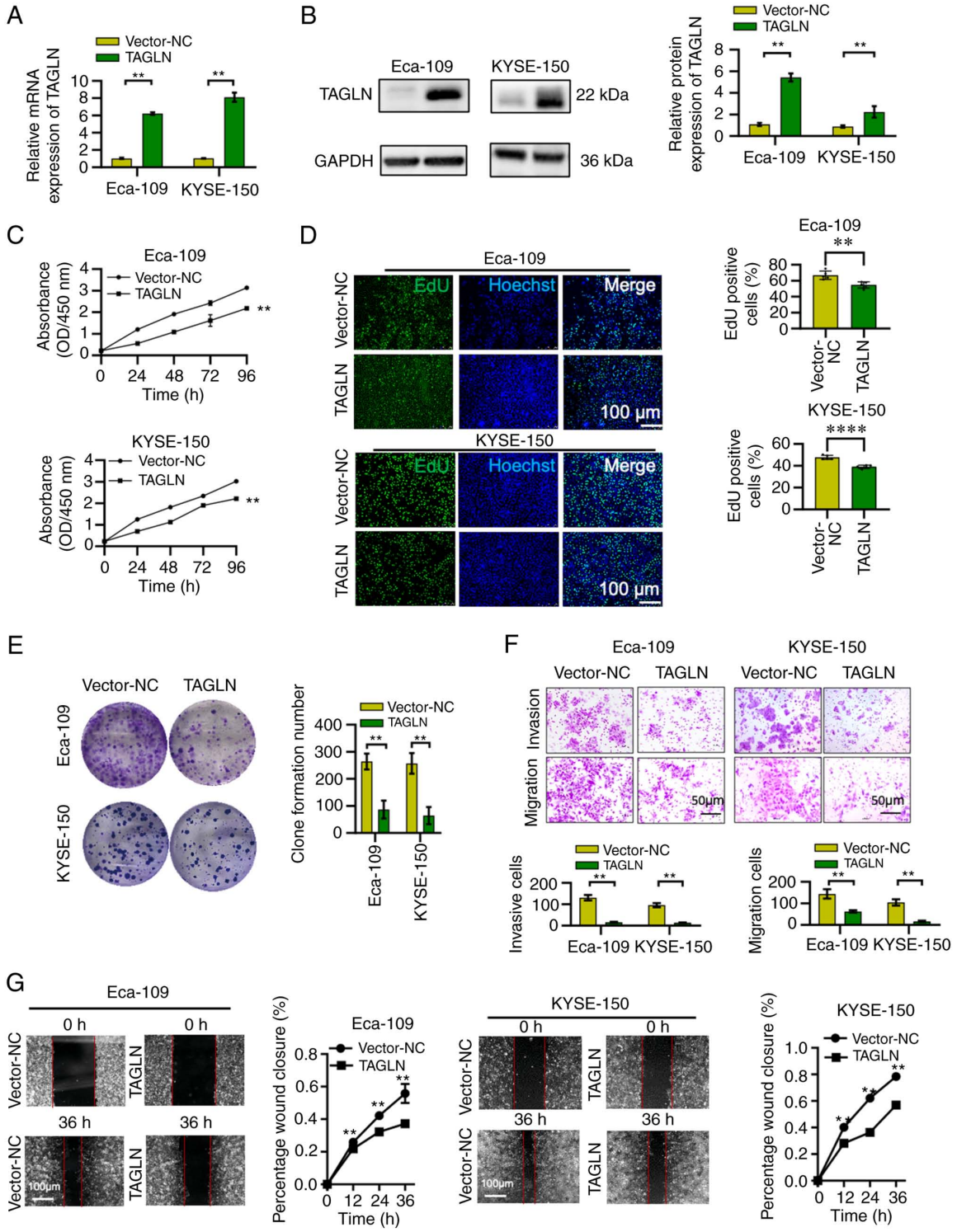

Figure 4. Overexpression of TAGLN diminishes proliferation, colony formation, invasion and migration in ESCC cells *in vitro*. Eca-109 and KYSE-150 cells were transfected with TAGLN overexpression plasmids and negative control plasmids. TAGLN expression was verified by (A) reverse transcription-quantitative PCR and (B) western blot. GAPDH was used as an internal control. The effects of TAGLN overexpression on the proliferation of Eca-109 and KYSE-150 cells was analyzed by (C) Cell Counting Kit-8 assay, (D) EdU and (E) colony formation assays. (F) Transwell invasion and migration assays were performed to determine the effects TAGLN overexpression in Eca-109 and KYSE-150 cells has on their invasive and migratory ability. (G) A wound healing assay was used to examine the effects TAGLN overexpression in Eca-109 and KYSE-150 cells migratory ability. Data are presented as the mean ± SD of three independent experiments. **P<0.01 vs. vector-NC, ****P<0.0001 as determined by two-tailed unpaired Student's t-test. ESCC, esophageal squamous cell carcinoma; NC, negative control; OD, optical density; TAGLN, transgelin.

TAGLN overexpression (Figs. 4G and S2). Taken together, these results demonstrated that the overexpression of TAGLN may attenuate the proliferation, colony formation, invasion and migration of the two ESCC cell lines.

Overexpression of TAGLN suppresses, whereas TAGLN knockdown promotes tumor growth in a xenograft model of ESCC. To investigate whether TAGLN serves a role in ESCC *in vivo*, a xenograft model was constructed. The inoculation

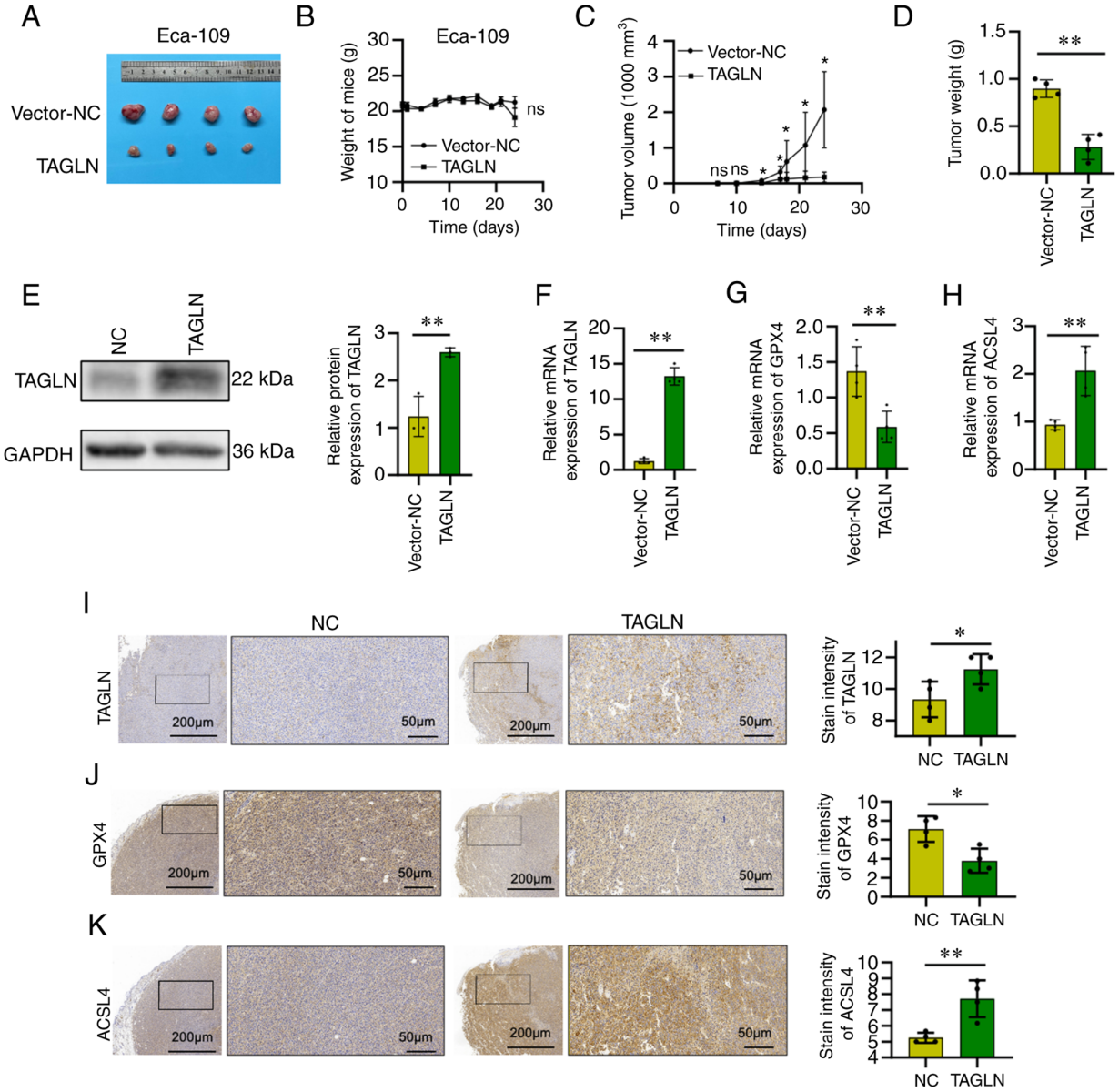

Figure 5. Overexpression of TAGLN suppresses tumor growth in xenograft models of esophageal squamous cell carcinoma. (A) Subcutaneous xenograft tumor images. (B) The whole-body weight of experiment nude mice remained unchanged. Compared with the control group, tumor (C) volume and (D) weight in TAGLN-Eca-109 cell treated mice was lower. (E) The expression of TAGLN in the excised tumors was verified by western blotting; GAPDH was used as an internal control. The mRNA expression levels of (F) TAGLN, (G) GPX4 and (H) ACSL4 were verified by reverse transcription-quantitative PCR. Representative immunohistochemical staining images of subcutaneous tumors revealed the staining intensity of (I) TAGLN, (J) GPX4 and (K) ACSL4 in the vector-NC and TAGLN-overexpression group. *P<0.05 and **P<0.001. ACSL4, acyl CoA synthetase long-chain family member 4; GPX4, glutathione peroxidase 4; NC, negative control; ns, not significant; TAGLN, transgelin.

of the mice with vector-NC or vector-TAGLN transfected Eca-109 cells revealed that TAGLN overexpression caused a marked reduction in tumor size, volume and weight after one month of growth compared with the mice inoculated with Eca-109-Vector-NC cells, whereas the whole-body weight of the mice remained the same (Fig. 5A-D). The TAGLN expression level of the subcutaneous tumors was subsequently assessed using western blot, RT-qPCR and immunohistochemical analyses, and the differences between vector-NC group and vector-TAGLN group were found to be statistically significant (Fig. 5E, F and I, respectively). Changes were also observed in the expression of the ferroptosis marker proteins, including GXP4 and ACSL4, in the subcutaneous tumors according to RT-qPCR and immunohistochemical analyses. GPX4 expression decreased, whereas that of ACSL4 increased, in the TAGLN-overexpression model mice compared with the control group (Fig. 5G, 5H, J and K). Taken together, these results suggested that the overexpression of TAGLN may cause a significant suppression of the progression of ESCC *in vivo*.

The injection of si-NC- or si-TAGLN-transfected Eca-109 cells into mice resulted in a significant increase in tumor volume and weight after one month of growth following TAGLN knockdown compared with the control Eca-109 cells (Fig. 6A, C and D, respectively), whereas the whole-body weight of the mice remained unchanged (Fig. 6B). Multiple tumor metastases were identified (and confirmed by H&E staining) in the livers of nude mice that were injected with si-TAGLN-transfected Eca-109 cells; the number of

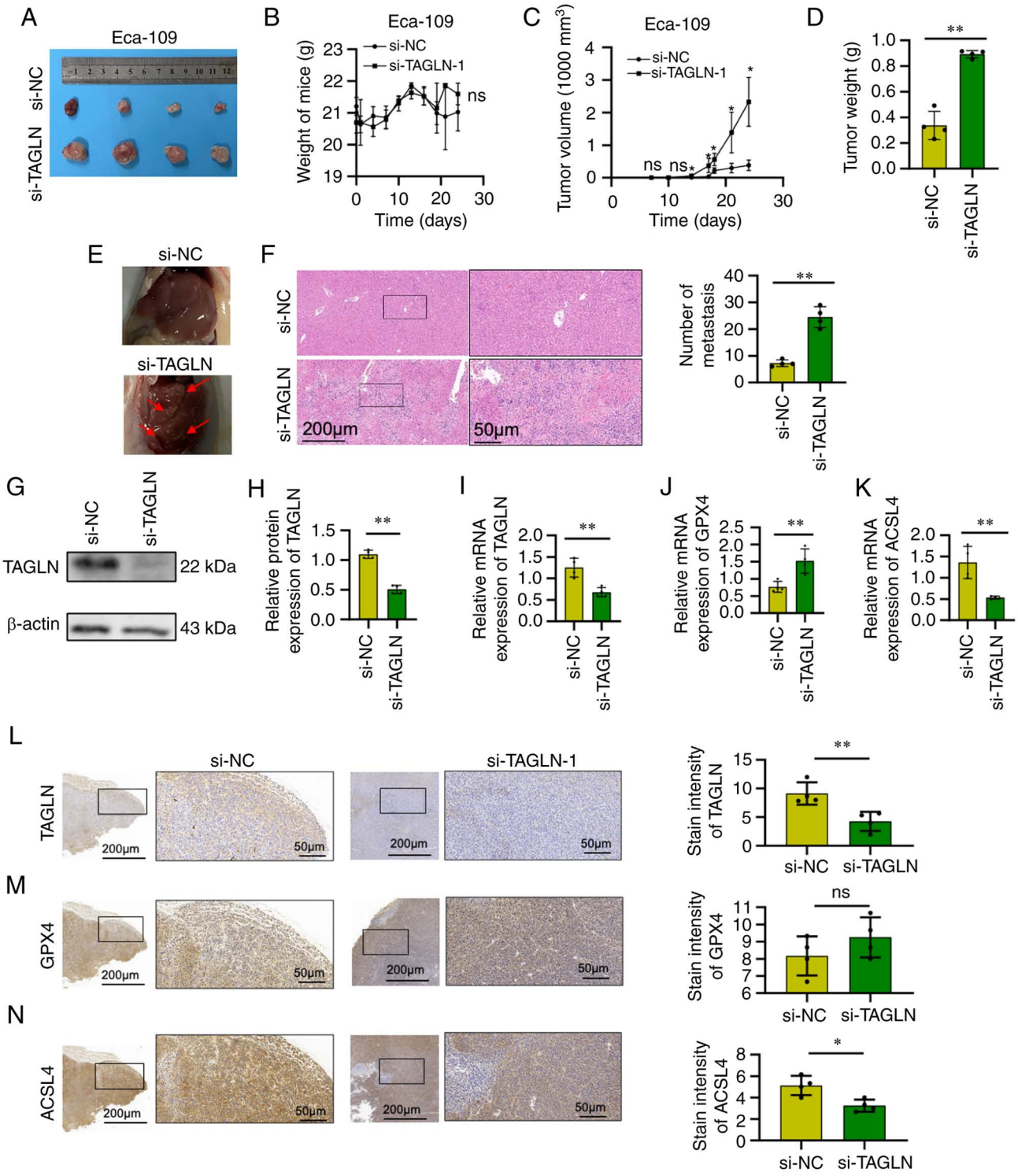

Figure 6. Knockdown of TAGLN promotes tumor growth in xenograft models of esophageal squamous cell carcinoma. (A) Subcutaneous xenograft tumor images. (B) The whole-body weight of experiment nude mice remained unchanged. Tumor (C) volume and (D) weight increased in si-TAGLN-Eca-109 cells treated mice compared with the control group. (E) Representative images of liver metastatic tumors. (F) H&E staining of liver metastatic tumors. (G and H) The protein expression level of TAGLN was semi-quantified by western blotting; GAPDH was used as an internal control. The mRNA expression levels of (I) TAGLN, (J) GPX4 and (K) ACSL4 were verified by reverse transcriptase-quantitative PCR. Representative immunohistochemical staining images of subcutaneous tumors revealed the relative staining levels of (L) TAGLN, (M) GPX4 and (N) ACSL4 in the si-NC and si-TAGLN groups. *P<0.05 and **P<0.001. ACSL4, acyl CoA synthetase long-chain family member 4; GPX4, glutathione peroxidase 4; NC, negative control; ns, not significant; si, small interfering RNA; TAGLN, transgelin.

metastases was found to be significantly higher compared with the control group (Fig. 6E and F). The expression level of TAGLN in the subcutaneous tumors was detected by western blot, RT-qPCR and immunohistochemical analyses, and the expression was found to be significantly decreased compared with the control group (Fig. 6G-I and L). In addition, changes were also observed in the expression of the ferroptosis marker proteins, GXP4 and ACSL4, in the subcutaneous tumors using

RT-qPCR and immunohistochemical analyses. According to RT-qPCR, compared with the control group, the expression of GPX4 was increased, whereas that of ACSL4 was decreased, following the knockdown of TAGLN (Fig. 6J and K). However, according to IHC staining, the difference of GPX4 expression between si-NC and si-TAGLN was not statistically significant, whereas that of ACSL4 was decreased in si-TAGLN group compared with the control group, following the knockdown of TAGLN. (Fig. 6M and N).

Investigation of the mechanism of TAGLN in inhibiting the malignant progression of ESCC through ferroptosis. Transcriptome analysis results demonstrated significant differential normalized transcripts per million and gene expression in the vector-NC and TAGLN-overexpression Eca-109 cells (Figs. 7A and B, and S3). To screen the differentially expressed genes, GO and KEGG enrichment analyses were performed (Fig. 7C). The analysis of GO enrichment showed that the BP and MF subontology were differentially regulated in TAGLN-overexpressing Eca-109 cells. For GO-BP, this regulation was associated with 'metal ion transport', 'dynamin family protein polymerization related to mitochondrial fission', 'epithelial cell apoptotic process', 'regulation of amino acid import across plasma membrane', and 'blood vessel endothelial cell proliferation in angiogenesis'. The overexpression of TAGLN induced the regulation of GO-MF gene categories associated with 'dynein intermediate chain binding', 'divalent inorganic cation transmembrane transporter activity', 'transition metal ion transmembrane transporter activity', 'ion transmembrane transporter activity' and 'protein serine/threonine phosphatase activity'. KEGG analysis showed that the overexpression of TAGLN regulated various pathways, including 'oxidative phosphorylation', 'transcriptional misregulation in cancer', 'TGF-β signaling pathway', 'signaling pathways regulating pluripotency of stem cells', 'pathways in cancer' and the 'PI3K-Akt signaling pathway'. These results indicated that TAGLN may contribute to the processes of oxidative phosphorylation, metal iron ion transport and cell apoptosis, leading to the occurrence of ferroptosis in ESCC cells and the inhibition of cancer proliferation, invasion and metastasis, together with associated signaling pathways. Moreover, the STRING tool was used to analyze the PPI networks of the TAGLN protein to determine their interaction in the progression of ESCC (Fig. 7D and E). As the results show, the crossover gene between PPI network and ferroptosis-related genes was GPX4, an essential protein of ferroptosis. These data suggested that TAGLN may regulate ferroptosis.

Overexpression of TAGLN promotes ferroptosis and regulates the expression of ferroptosis marker proteins. Western blot analysis was used to determine the expression levels of the ferroptosis marker proteins, GPX4 and ACSL4, following TAGLN overexpression. The protein expression level of ACSL4 was significantly increased, whereas that of GPX4 was significantly decreased, in Eca-109 and KYSE-150 cell lines following TAGLN overexpression compared with the vector-NC group (Fig. 8A). Furthermore, RT-qPCR results showed that the mRNA expression level of GPX4 in both ESCC cell lines was significantly decreased, whereas the expression level of ACSL4 was significantly increased (Fig. 8B). The overexpression of TAGLN caused a significant increase in the intracellular concentrations of MDA and lipid ROS (Fig. 8C and D, respectively), and a decrease in the concentration of GSH (Fig. 8E), suggesting that the overexpression of TAGLN may induce sensitivity to and promote ferroptosis. Levels of intracellular total iron (Fig. 8F) and Fe^{2+} iron (Fig. 8G and H) increased in Eca-109 and KYSE-150 cells overexpressing TAGLN compared with the vector-NC transfected groups. Taken together, these results suggested that TAGLN may serve a crucial oncogenic function in cancer progression by regulating ferroptosis in ESCC cells.

TAGLN regulates ferroptosis by interacting with p53. p53, one of the main factors that regulate ferroptosis, was identified from the intersection of the TAGLN interacting gene. Therefore, the functional interaction between TAGLN and p53 was selected for further investigation to unravel the molecular mechanism and metabolism of the malignancy in ESCC.RT-qPCR analysis revealed that the mRNA expression level of p53 significantly increased with an upregulation of TAGLN expression in Eca-109 cells (Fig. 9A). To investigate a putative interaction of TAGLN with p53, Co-IP and fluorescence co-localization experiments were conducted in Eca-109 cells (Fig. 9B and C, respectively). As Fig. 9C shown, TAGLN and p53 were both found to be abundant in the vector-TAGLN Eca-109 cell cytoplasm. These results indicated that TAGLN interacts with p53 and suggested that TAGLN may regulate ferroptosis through interacting with p53 in ESCC cells. Taken together, these results suggested that TAGLN inhibits the malignant progression and regulates ferroptosis by interacting with p53 in ESCC cells (Fig. 9D).

Discussion

Esophageal cancer has a relatively low 5-year overall survival rate of ~20% in Europe, USA and China (7); ESCC, the major subtype of esophageal cancer, has a higher incidence among Eastern Asian and Eastern and Southern African populations compared with the worldwide population (42). The aim of the present study was to suggested potential options for future therapeutic targets.

TAGLN is an actin-binding protein that stabilizes actin *in vitro* and is widely expressed in muscle tissue and organs, such as GI tract and heart (43-45). TAGLN may also be associated with cell migration, thereby promoting an invasive and malignant nature in cells (46). Previous studies have suggested that TAGLN has tumor-suppressive functions in certain cells that are not associated with the cytoskeleton *per se* (47,48). TAGLN expression was found to be significantly lower in bladder, breast and renal cell carcinoma tissues compared with matched normal tissues (49,50). TAGLN expression was shown to be markedly reduced in colorectal cancer samples compared with normal colorectal mucosa, and this was associated with poor overall survival in patients with colorectal cancer (50). In prostate carcinoma cells, TAGLN was found to block androgen-stimulated cell growth by inhibiting the binding of an androgen receptor co-activator with its androgen receptor (51). These studies indicated that the loss of

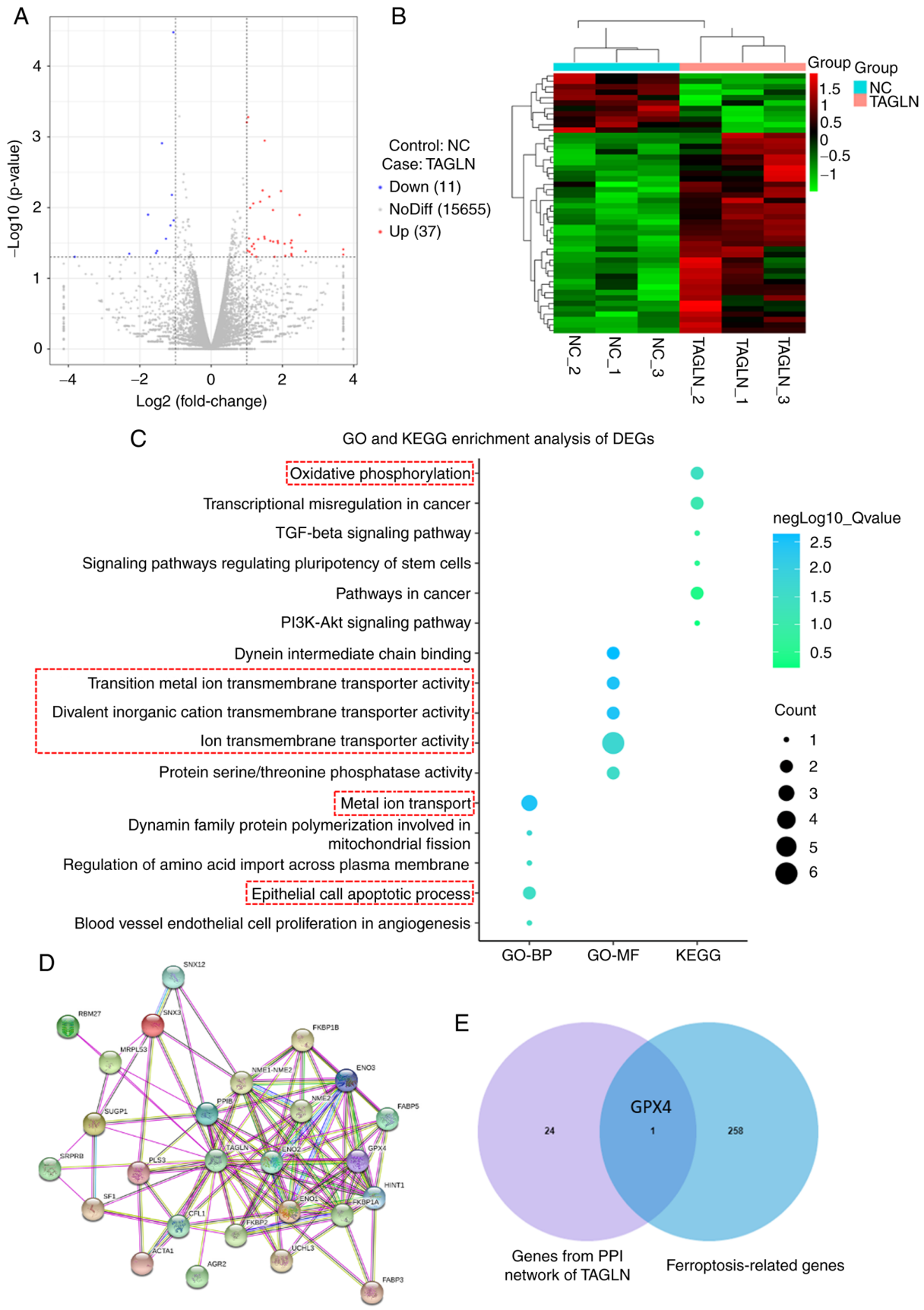

Figure 7. Mechanism of TAGLN inhibition of esophageal squamous cell carcinoma progression by ferroptosis. DEGs were identified in Eca-109 cells transfected with vector-NC or TAGLN-overexpression plasmid. (A) Volcano plot and (B) cluster heatmap showing the results of differential analyses in the two groups. (C) Analysis of GO-BP, GO-MF and KEGG enrichment analyses showed the differential regulation of gene categories induced by the overexpression of TAGLN. (D) Using STRING tool to analyze the PPI network of TAGLN protein, p53, one of the main factors that regulate ferroptosis, was identified from the intersection of the TAGLN interacting genes. (E) The Venn diagram between genes from PPI network and ferroptosis-related genes. DEG, differentially expressed gene; GO, Gene Ontology; GPX4, glutathione peroxidase 4; KEGG, Kyoto Encyclopedia of Genes and Genomes; NC, negative control; TAGLN, transgelin.

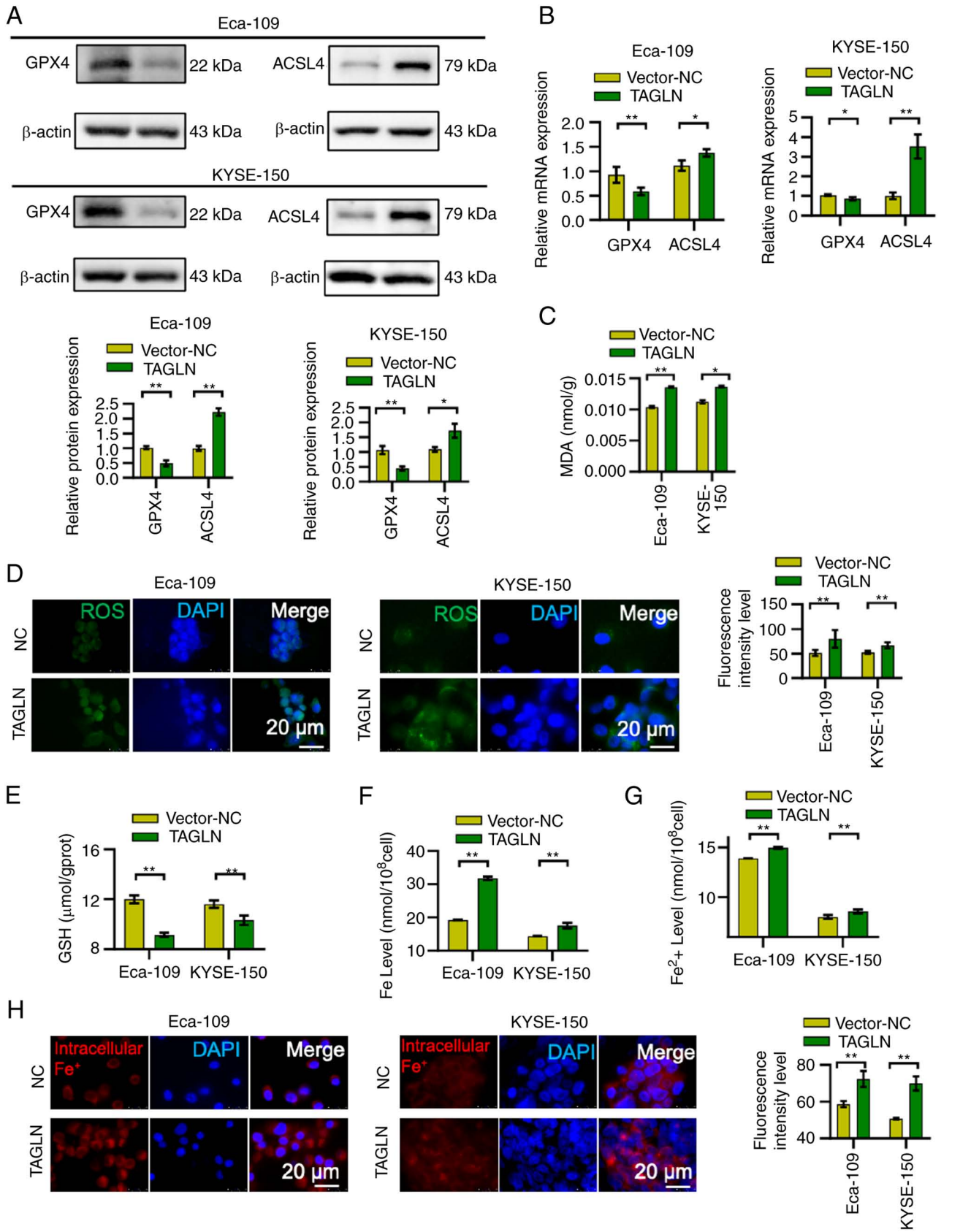

Figure 8. Overexpression of TAGLN promotes ferroptosis and regulates ferroptosis marker proteins expression. The (A) protein and (B) mRNA expression levels of ferroptosis marker proteins, GPX4 and ACSL4, were verified by western blotting (β-actin was used as the internal control) and reverse transcription-quantitative PCR, respectively. Intracellular concentrations of (C) MDA and (D) lipid ROS increased, whereas (E) GSH decreased in Eca-109 and KYSE-150 cells overexpressing TAGLN compared with the vector-NC groups. Levels of (F) intracellular total iron, (G) ferrous iron and (H) intracellular Fe^{2+} iron increased in Eca-109 and KYSE-150 cells overexpressing TAGLN compared with the vector-NC groups. Data are shown as the mean ± SD of three independent experiments. *P<0.05 and **P<0.01, as determined by two-tailed unpaired Student's t-test. ACSL4, acyl CoA synthetase long-chain family member 4; CCK-8, Cell Counting Kit-8; fer, ferrostatin; GPX4, glutathione peroxidase 4; GSH, glutathione; NC, negative control; ROS, reactive oxygen species; TAGLN, transgelin.

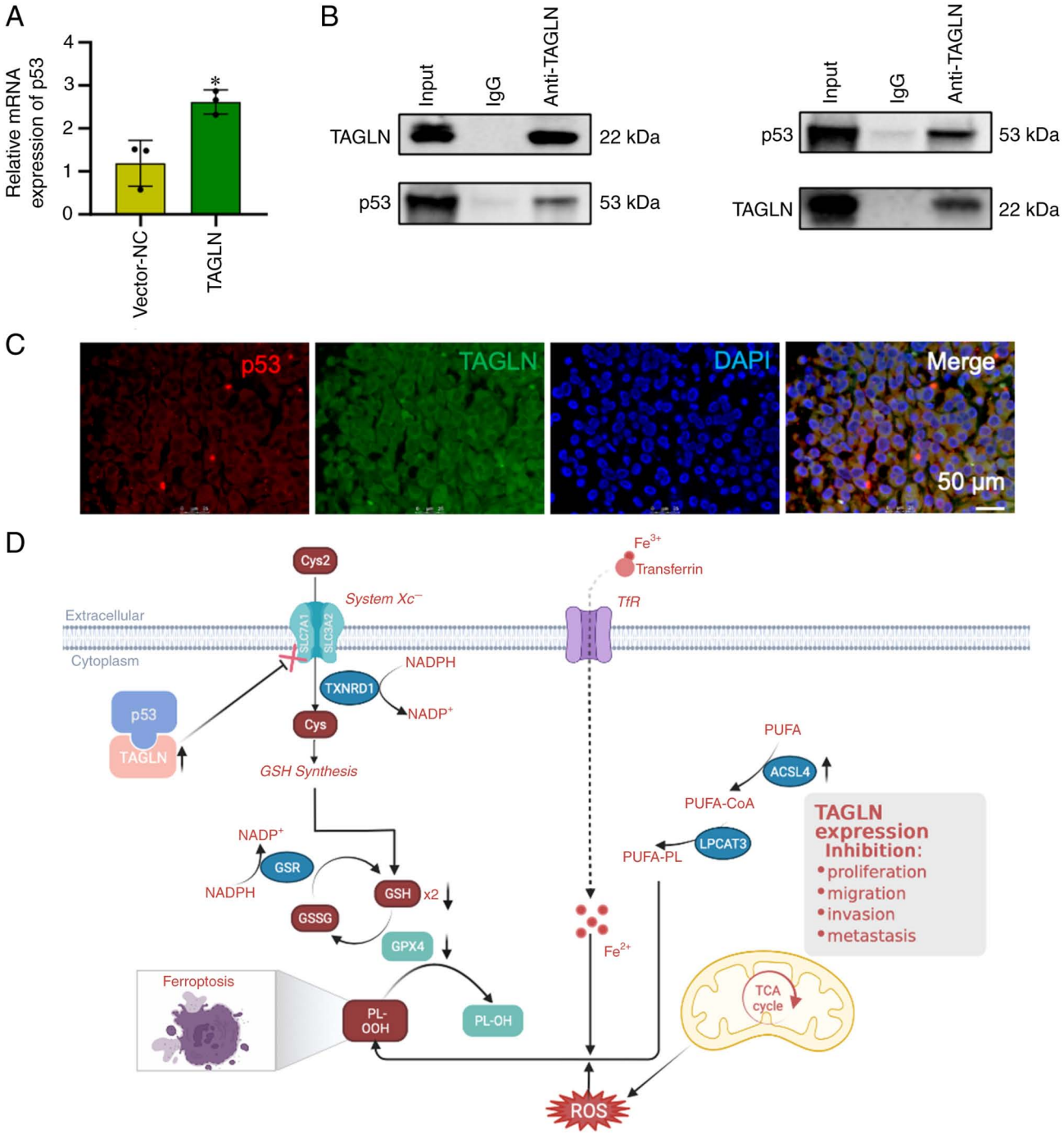

Figure 9. TAGLN regulates ferroptosis by interacting with p53. (A) The mRNA expression of p53 in TAGLN overexpressing cells was verified by reverse transcription-quantitative PCR in Eca-109 cell line. (B) Co-immunoprecipitation results indicated that TAGLN coimmunoprecipitated with p53 and p53 coimmunoprecipitated with TAGLN in Eca-109 cell line. (C) Fluorescence co-localization results showed that p53 and TAGLN are present in the Eca-109 cytoplasm. (D) Mechanism of TAGLN/p53 inhibition of the malignant progression, including proliferation, migration, invasion and metastasis, of ESCC cells by regulating ferroptosis as evidenced by downregulation of GPX4, reduced GSH levels, increased ROS and increased intracellular iron level. *P<0.05.

TAGLN gene expression may be an event in malignant tumor progression. In our previous study, TAGLN expression was shown to inhibited ESCC progression, and that, through inhibiting the occurrence of EMT, it may ultimately be possible to prevent the malignant progression of ESCC (34). According to results from the present study, TAGLN may have an important role in the malignant progression of ESCC. A longer overall survival rate was observed in patients who had higher levels of TAGLN expression. The level of TAGLN expression in ESCC tissues may also be beneficial in terms of clinically evaluating the degree of the malignancy and the prognosis of patients with ESCC. Thus, another aim of the present study was to further investigate the role of TAGLN in ESCC and to explore the underlying mechanism.

According to the GSEA analysis performed in the present study, TAGLN may be able to influence several pathways that are linked with ESCC cell functions and tumor characteristics. Focal adhesions, ECM-receptor interactions, gap junction and

CAMs are the factors/processes that affect tumor invasion. TAGLN can also affect the NER process that is associated with cancer. The TGF-β signaling pathway, a tumor immune regulatory pathway, was also found to be associated with the expression level of TAGLN in ESCC. Based on these findings, it was possible to speculate that TAGLN may be a tumor suppressor in ESCC that inhibits the invasion of ESCC, and possibly the progression of other malignancies, through tumor immune pathways. Subsequently, *in vitro* and *in vivo* experiments were performed to verify the above results. The data obtained indicated that increased TAGLN expression caused an attenuation of the malignancy of Eca-109 and KYSE-150 cells, whereas the downregulation of TAGLN enhanced the ability of ESCC cells to proliferate, migrate and invade. The malignancy of the Eca-109 and KYSE-150 cells was impacted by TAGLN expression, and these results suggested that the overexpression of TAGLN in ESCC cell lines both promoted ferroptosis and regulated the expression of ferroptosis marker proteins.

The results of the transcriptome analysis in the current study revealed the association between TAGLN expression and the GO-BP and GO-MF subontologies associated with ion accumulation and programmed cell death during ferroptosis (52-54). In addition, the findings further confirmed that TAGLN may contribute to oxidative phosphorylation, Fe^{2+} transport and apoptosis, leading to the occurrence of ferroptosis in ESCC cells, as well as the inhibition of cancer cell proliferation, invasion, metastasis and the associated signaling pathways. p53 is one of the main factors that regulate ferroptosis (16,51). Subsequently, the STRING tool analysis of the PPI networks of the TAGLN showed that p53 may interact with TAGLN. RT-qPCR results confirmed that the p53 expression increased concomitantly with the overexpression of TAGLN. Moreover, the protein interactions between p53 and TAGLN in the ESCC cell lines were verified by Co-IP and immunofluorescence co-localization staining experiments. According to previous studies (55,56), TAGLN may promotes ferroptosis and inhibits the malignant evolution of ESCC through interacting with p53. Tsui *et al* (55) reported that TAGLN expression was higher in bladder smooth muscle, fibroblast and normal epithelial cells compared with carcinoma cells *in vitro*. The findings suggested that TAGLN is a p53 upregulated gene; ectopic overexpression of p53 induced TAGLN expression and, further, TAGLN was shown to inhibit cell proliferation and invasion *in vitro* and block tumorigenesis *in vivo*. Zhang *et al* (56) reported that overexpression of TAGLN resulted in both an increase in the cytoplasmic translocation of p53 and the upregulation of p53 expression in prostate cancer cell lines. The interplay between TAGLN and p53 *in vivo*, and triggering of the mitochondria-associated apoptotic pathway were detected in the lymph node carcinoma of the prostate cells following transfection with TAGLN.

Unlimited lipid peroxidation and a rupture of the plasma membrane cause ferroptosis (20), which can be stimulated through extrinsic and intrinsic pathways (57). A blockade of intracellular antioxidant enzymes (such as GPX4) activates the intrinsic pathway (16,58). The suppression of cell membrane transporters, such as the cystine/glutamate transporter (also known as system xc-), or the stimulation of iron transporters, such as serotransferrin and lactotransferrin, are two ways in which the extrinsic pathway can be activated (59). System xc- is comprised of SLC7A11 and SLC3A2 subunits. Both the activity and expression level of SLC7A11 are negatively regulated by tumor suppressor genes, such as p53 (60). Ferroptosis in cancer cells is promoted by the p53-mediated transcriptional inhibition of SLC7A11, and the ability of p53 to promote apoptosis and ferroptosis is altered by changes in p53 (mutations or polymorphisms) (61). Although, in lung cancer cell lines, the ability of the $p53^{3KR}$ acetylation-defective mutant to induce ferroptosis is retained, it is not able to induce apoptosis (17). In summary, it is possible to speculate that TAGLN promotes ferroptosis by interacting with p53 in ESCC.

In conclusion, the present study demonstrated that TAGLN may prevent the proliferation, migration, invasion and metastasis of ESCC through regulating the occurrence of ferroptosis. ESCC is difficult to diagnose at an early stage. At present, effective treatment methods are lacking, and the prognosis of ESCC is poor. For these reasons, it is essential to design and perform additional studies that focus on the incidence, development and metastasis of ESCC. Recently, TAGLN has been found to have a role in various types of tumor, although its biological function(s) and the underlying mechanism(s) remain poorly understood (62). Our previous study demonstrated that TAGLN inhibited ESCC and regulated EMT in ESCC (34). The present study demonstrated that the expression level of TAGLN is low in ESCC, and that the expression level of ESCC is associated with prognostic characteristics. The expression of TAGLN was significantly associated with the stage and grade of ESCC, and the overall survival of patients with ESCC. In this study, the inhibitory effect of TAGLN on ESCC was verified by more phenotypic experiments such as EdU, colony formation and nude mice xenograft assays. We hypothesized that the inhibitory effect of TAGLN on ESCC is not accomplished by EMT alone. By bioinformatics analysis and the detection of ferroptosis indicators in ESCC patients, it was found that TAGLN may regulate ferroptosis through p53 and, thus, inhibit ESCC. In addition, the number of cases included in this study is small and the sample size is small, so it has certain limitations. The sample size will be expanded for further verification in the future. Finally, the present study has demonstrated that, regulating ferroptosis may become a new direction of tumor therapy, and it also suggested that TAGLN may be a therapeutic target for ESCC.

Acknowledgements

Not applicable.

Funding

The present study was financially supported by The National Natural Science Foundation of China (grant nos. 82000511, 82170558 and 81900487), Scientific and Technological Projects of Tianjin (grant no. 21JCQNJC01120), Health Science and Technology Project of Tianjin (grant no. TJWJ2021QN006), Scientific Research Project of Tianjin Education Commission (grant no. 2019KJ197), Tianjin Science and Technology Plan Project (grant no. 21JCQNJC00990), Health Commission of Shanxi Province Science and Technology Guiding Project (grant no. 2021XM40), Basic Research Program

of Shanxi Provincial Science and Technology Department (grant no. 20210302123013) and Key Technology Research and Development Project of Jincheng Science and Technology Bureau (grant no. 20210118).

Availability of data and materials

The datasets used and/or analyzed in the current study are available from the corresponding author on reasonable request. Transcriptome analysis of original data were uploaded to the NCBI database, and accession to cite for these SRA data is PRJNA924358 (https://www.ncbi.nlm.nih.gov/sra/PRJNA924358).

Authors' contributions

WZ and BW designed the study. WZ, QC, BY, LZ, CW, XK, XX, YG, XL, QD, LZ, YL and CW performed the experiments and analyzed the data. QC, CW and WZ performed the data analysis. QC and WZ wrote the initial draft of the paper, with contributions from all authors. All authors have read and approved the final manuscript.

Ethics approval and consent to participate

Written informed consent was provided by each patient, and the Ethics Committee of Tianjin Medical University General Hospital (Tianjin, China) approved the study (ethics no. IRB2021 WZ 134). The animal study was approved by the Ethics Committee of Tianjin Medical University General Hospital (ethics no. IRB2019-DWFL-414).

Patient consent for publication

Not applicable.

Competing interests

The authors declare that they have no competing interests.

References

1. Ferlay J, Ervik M, Lam F, Colombet M, Mery L, Piñeros M, Znaor A, Soerjomataram I, Bray F: Global Cancer Observatory: Cancer Today. International Agency for Research on Cancer, Lyon, 2020. https://gco.iarc.fr/today. Accessed December 20, 2022.
2. Waters JK and Reznik SI: Update on management of squamous cell esophageal cancer. Curr Oncol Rep 24: 375-385, 2022.
3. Bray F, Ferlay J, Soerjomataram I, Siegel RL, Torre LA and Jemal A: Global cancer statistics 2018: GLOBOCAN estimates of incidence and mortality worldwide for 36 cancers in 185 countries. CA Cancer J Clin 68: 394-424, 2018.
4. Arnold M, Ferlay J, van Berge Henegouwen MI and Soerjomataram I: Global burden of oesophageal and gastric cancer by histology and subsite in 2018. Gut 69: 1564-1571, 2020.
5. Fitzmaurice C, Abate D, Abbasi N, Abbastabar H, Abd-Allah F, Abdel-Rahman O, Abdelalim A, Abdoli A, Abdollahpour I, Abdulle ASM, *et al*: Global, regional, and national cancer incidence, mortality, years of life lost, years lived with disability, and disability-adjusted life-years for 29 cancer groups, 1990 to 2017: A systematic analysis for the global burden of disease study. JAMA Oncol 5: 1749-1768, 2019.
6. Pan R, Zhu M, Yu C, Lv J, Guo Y, Bian Z, Yang L, Chen Y, Hu Z, Chen Z, *et al*: Cancer incidence and mortality: A cohort study in China, 2008-2013. Int J Cancer 141: 1315-1323, 2017.
7. Lagergren J, Smyth E, Cunningham D and Lagergren P: Oesophageal cancer. Lancet 390: 2383-2396, 2017.
8. Zeng H, Chen W, Zheng R, Zhang S, Ji JS, Zou X, Xia C, Sun K, Yang Z, Li H, *et al*: Changing cancer survival in China during 2003-15: A pooled analysis of 17 population-based cancer registries. Lancet Glob Health 6: e555-e567, 2018.
9. Lin DC, Hao JJ, Nagata Y, Xu L, Shang L, Meng X, Sato Y, Okuno Y, Varela AM, Ding LM, *et al*: Genomic and molecular characterization of esophageal squamous cell carcinoma. Nat Genet 46: 467-473, 2014.
10. Wu C, Wang Z, Song X, Feng XS, Abnet CC, He J, Hu N, Zuo XB, Tan W, Zhan Q, *et al*: Joint analysis of three genome-wide association studies of esophageal squamous cell carcinoma in Chinese populations. Nat Genet 46: 1001-1006, 2014.
11. Huang S, Guo Y, Li Z, Zhang Y, Zhou T, You W, Pan K and Li W: A systematic review of metabolomic profiling of gastric cancer and esophageal cancer. Cancer Biol Med 17: 181-198, 2020.
12. Chen X, Kang R, Kroemer G and Tang D: Broadening horizons: The role of ferroptosis in cancer. Nat Rev Clin Oncol 18: 280-296, 2021.
13. Liu J, Ren L, Li S, Li W, Zheng X, Yang Y, Fu W, Yi J, Wang J and Du G: The biology, function, and applications of exosomes in cancer. Acta Pharm Sin B 11: 2783-2797, 2021.
14. Chen X, Zhou Z, Zhang Z, Zhao C, Li J, Jiang J, Huang B and Qin Y: Puerarin inhibits EMT induced by oxaliplatin via targeting carbonic anhydrase XII. Front Pharmacol 13: 969422, 2022.
15. Yang WS, SriRamaratnam R, Welsch ME, Shimada K, Skouta R, Viswanathan VS, Cheah JH, Clemons PA, Shamji AF, Clish CB, *et al*: Regulation of ferroptotic cancer cell death by GPX4. Cell 156: 317-331, 2014.
16. Jiang L, Kon N, Li T, Wang SJ, Su T, Hibshoosh H, Baer R and Gu W: Ferroptosis as a p53-mediated activity during tumour suppression. Nature 520: 57-62, 2015.
17. Dixon SJ, Lemberg KM, Lamprecht MR, Skouta R, Zaitsev EM, Gleason CE, Patel DN, Bauer AJ, Cantley AM, Yang WS, *et al*: Ferroptosis: An iron-dependent form of nonapoptotic cell death. Cell 149: 1060-1072, 2012.
18. Torti SV, Manz DH, Paul BT, Blanchette-Farra N and Torti FM: Iron and cancer. Annu Rev Nutr 38: 97-125, 2018.
19. Chen X, Yu C, Kang R and Tang D: Iron metabolism in ferroptosis. Front Cell Dev Biol 8: 590226, 2020.
20. Stockwell BR, Angeli JP, Bayir H, Bush AI, Conrad M, Dixon SJ, Fulda S, Gascón S, Hatzios SK, Kagan VE, *et al*: Ferroptosis: A regulated cell death nexus linking metabolism, redox biology, and disease. Cell 171: 273-285, 2017.
21. Yang WS, Kim KJ, Gaschler MM, Patel M, Shchepinov MS and Stockwell BR: Peroxidation of polyunsaturated fatty acids by lipoxygenases drives ferroptosis. Proc Natl Acad Sci USA 113: E4966-E4975, 2016.
22. Feng L, Zhao K, Sun L, Yin X, Zhang J, Liu C and Li B: SLC7A11 regulated by NRF2 modulates esophageal squamous cell carcinoma radiosensitivity by inhibiting ferroptosis. J Transl Med 19: 367, 2021.
23. Cao JY and Dixon SJ: Mechanisms of ferroptosis. Cell Mol Life Sci 73: 2195-2209, 2016.
24. Linkermann A, Skouta R, Himmerkus N, Mulay SR, Dewitz C, De Zen F, Prokai A, Zuchtriegel G, Krombach F, Welz PS, *et al*: Synchronized renal tubular cell death involves ferroptosis. Proc Natl Acad Sci USA 111: 16836-16841, 2014.
25. Doll S, Proneth B, Tyurina YY, Panzilius E, Kobayashi S, Ingold I, Irmler M, Beckers J, Aichler M, Walch A, *et al*: ACSL4 dictates ferroptosis sensitivity by shaping cellular lipid composition. Nat Chem Biol 13: 91-98, 2017.
26. Kenny EM, Fidan E, Yang Q, Anthonymuthu TS, New LA, Meyer EA, Wang H, Kochanek PM, Dixon CE, Kagan VE and Bayir H: Ferroptosis contributes to neuronal death and functional outcome after traumatic brain injury. Crit Care Med 47: 410-418, 2019.
27. Zhong W, Sun B, Gao W, Qin Y, Zhang H, Huai L, Tang Y, Liang Y, He L, Zhang X, *et al*: Salvianolic acid A targeting the transgelin-actin complex to enhance vasoconstriction. EBioMedicine 37: 246-258, 2018.
28. Wen F, Sun X, Sun C, Dong Z, Jia G, Bao W, Yu H and Yang C: TAGLN is downregulated by TRAF6-mediated proteasomal degradation in prostate cancer cells. Mol Cancer Res 19: 1113-1122, 2021.
29. Xi Y, Liu J and Shen G: Low expression of IGFBP4 and TAGLN accelerate the poor overall survival of osteosarcoma. Sci Rep 12: 9298, 2022.
30. Sayar N, Karahan G, Konu O, Bozkurt B, Bozdogan O and Yulug IG: Transgelin gene is frequently downregulated by promoter DNA hypermethylation in breast cancer. Clin Epigenetics 7: 104, 2015.

31. Yu B, Chen X, Li J, Qu Y, Su L, Peng Y, Huang J, Yan J, Yu Y, Gu Q, *et al*: Stromal fibroblasts in the microenvironment of gastric carcinomas promote tumor metastasis via upregulating TAGLN expression. BMC Cell Biol 14: 17, 2013.
32. Wu X, Dong L, Zhang R, Ying K and Shen H: Transgelin over-expression in lung adenocarcinoma is associated with tumor progression. Int J Mol Med 34: 585-591, 2014.
33. Zhou L, Zhang R, Zhang L, Sun Y, Yao W, Zhao A, Li J and Yuan Y: Upregulation of transgelin is an independent factor predictive of poor prognosis in patients with advanced pancreatic cancer. Cancer Sci 104: 423-430, 2013.
34. Zhong W, Hou H, Liu T, Su S, Xi X, Liao Y, Xie R, Jin G, Liu X, Zhu L, *et al*: Cartilage oligomeric matrix protein promotes epithelial-mesenchymal transition by interacting with Transgelin in colorectal cancer. Theranostics 10: 8790-8806, 2020.
35. Yang B, Chen Q, Wan C, Sun S, Zhu L, Zhao Z, Zhong W and Wang B: Transgelin inhibits the malignant progression of esophageal squamous cell carcinomas by regulating epithelial-mesenchymal transition. Front Oncol 11: 709486, 2021.
36. Rice TW, Kelsen D, Blackstone EH, Ishwaran H and Hofstetter WL: Esophagus and Esophagogastric Junction. 2017. AJCC Cancer Staging Manual.
37. Nicchia GP, Stigliano C, Sparaneo A, Rossi A, Frigeri A and Svelto M: Inhibition of aquaporin-1 dependent angiogenesis impairs tumour growth in a mouse model of melanoma. J Mol Med (Berl) 91: 613-623, 2013.
38. Simone L, Gargano CD, Pisani F, Cibelli A, Mola MG, Frigeri A, Svelto M and Nicchia GP: Aquaporin-1 inhibition reduces metastatic formation in a mouse model of melanoma. J Cell Mol Med 22: 904-912, 2018.
39. Boren T, Xiong Y, Hakam A, Wenham R, Apte S, Wei Z, Kamath S, Chen DT, Dressman H and Lancaster JM: MicroRNAs and their target messenger RNAs associated with endometrial carcinogenesis. Gynecol Oncol 110: 206-215, 2008.
40. Najafi M, Farhood B and Mortezaee K: Extracellular matrix (ECM) stiffness and degradation as cancer drivers. J Cell Biochem 120: 2782-2790, 2019.
41. Murphy JM, Rodriguez Y, Jeong K, Ahn EE and Lim SS: Targeting focal adhesion kinase in cancer cells and the tumor microenvironment. Exp Mol Med 52: 877-886, 2020.
42. Abnet CC, Arnold M and Wei WQ: Epidemiology of esophageal squamous cell carcinoma. Gastroenterology 154: 360-373, 2018.
43. Lees-Miller JP, Heeley DH and Smillie LB: An abundant and novel protein of 22 kDa (SM22) is widely distributed in smooth muscles. Purification from bovine aorta. Biochem J 244: 705-709, 1987.
44. Camoretti-Mercado B, Forsythe SM, LeBeau MM, Espinosa R III, Vieira JE, Halayko AJ, Willadsen S, Kurtz B, Ober C, Evans GA, *et al*: Expression and cytogenetic localization of the human SM22 gene (TAGLN). Genomics 49: 452-457, 1998.
45. Lawson D, Harrison M and Shapland C: Fibroblast transgelin and smooth muscle SM22alpha are the same protein, the expression of which is down-regulated in many cell lines. Cell Motil Cytoskeleton 38: 250-257, 1997.
46. Ueda T, Araki N, Mano M, Myoui A, Joyama S, Ishiguro S, Yamamura H, Takahashi K, Kudawara I and Yoshikawa H: Frequent expression of smooth muscle markers in malignant fibrous histiocytoma of bone. J Clin Pathol 55: 853-858, 2002.
47. Gimona M, Kaverina I, Resch GP, Vignal E and Burgstaller G: Calponin repeats regulate actin filament stability and formation of podosomes in smooth muscle cells. Mol Biol Cell 14: 2482-2491, 2003.
48. Wei X, Lou H, Zhou D, Jia Y, Li H, Huang Q, Ma J, Yang Z, Sun C, Meng Y, *et al*: TAGLN mediated stiffness-regulated ovarian cancer progression via RhoA/ROCK pathway. J Exp Clin Cancer Res 40: 292, 2021.
49. Rao D, Kimler BF, Nothnick WB, Davis MK, Fan F and Tawfik O: Transgelin: A potentially useful diagnostic marker differentially expressed in triple-negative and non-triple-negative breast cancers. Hum Pathol 46: 876-883, 2015.
50. Assinder SJ, Stanton JA and Prasad PD: Transgelin: An actin-binding protein and tumour suppressor. Int J Biochem Cell Biol 41: 482-486, 2009.
51. Thompson O, Moghraby JS, Ayscough KR and Winder SJ: Depletion of the actin bundling protein SM22/transgelin increases actin dynamics and enhances the tumourigenic phenotypes of cells. BMC Cell Biol 13: 1, 2012.
52. Yang Z, Chang YJ, Miyamoto H, Ni J, Niu Y, Chen Z, Chen YL, Yao JL, di Sant'Agnese PA and Chang C: Transgelin functions as a suppressor via inhibition of ARA54-enhanced androgen receptor transactivation and prostate cancer cell growth. Mol Endocrinol 21: 343-358, 2007.
53. Li J, Cao F, Yin HL, Huang ZJ, Lin ZT, Mao N, Sun B, Wang G: Ferroptosis: Past, present and future. Cell Death Dis 11: 88, 2020.
54. Li Y, Zeng X, Lu D, Yin M, Shan M and Gao Y: Erastin induces ferroptosis via ferroportin-mediated iron accumulation in endometriosis. Hum Reprod 36: 951-964, 2021.
55. Tsui KH, Lin YH, Chang KS, Hou CP, Chen PJ, Feng TH and Juang HH: Transgelin, a p53 and PTEN-upregulated gene, inhibits the cell proliferation and invasion of human bladder carcinoma cells in vitro and in vivo. Int J Mol Sci 20: 4946, 2019.
56. Zhang ZW, Yang ZM, Zheng YC and Chen ZD: Transgelin induces apoptosis of human prostate LNCaP cells through its interaction with p53. Asian J Androl 12: 186-195, 2010.
57. Tang D and Kroemer G: Ferroptosis. Curr Biol 30: R1292-R1297, 2020.
58. Lei G, Zhuang L and Gan B: Targeting ferroptosis as a vulnerability in cancer. Nat Rev Cancer 22: 381-396, 2022.
59. Liu MR, Zhu WT and Pei DS: System Xc(-): A key regulatory target of ferroptosis in cancer. Invest New Drugs 39: 1123-1131, 2021.
60. Koppula P, Zhuang L and Gan B: Cystine transporter SLC7A11/xCT in cancer: Ferroptosis, nutrient dependency, and cancer therapy. Protein Cell 12: 599-620, 2021.
61. Gong D, Chen M, Wang Y, Shi J and Hou Y: Role of ferroptosis on tumor progression and immunotherapy. Cell Death Discov 8: 427, 2022.
62. Zhou Y, Bian S, Zhou X, Cui Y, Wang W, Wen L, Guo L, Fu W and Tang F: Single-cell multiomics sequencing reveals prevalent genomic alterations in tumor stromal cells of human colorectal cancer. Cancer Cell 38: 818-828.e5, 2020.